a.

```
AtphotI-LOV1(aa171-308)    171: DGDVPGGRSGIPRVSEDLKDALSTFGQIFVVSDATKPDYPIMYASAGFFNMTGYTSKEVV  230
AtphotI-LOV2(aa449-586)    449: ESVDDKVRQKEMNRKGIDLATTLERIEKNFVITDPRLPDNPIIFASDSFLELTEYSREEIL  508
Atphot2-LOV1(aa107-244)    107: EESTSSESGAFPRVSQELKTALSTLQQTFVVSDATQPHCPIVYASSGFFTMTGYSSKEIV  166
Atphot2-LOV2(aa363-500)    363: DSVDLSDRERDIRQGIDLATTLERIEKNFVISDPRLPDNPIIFASDSFLELTEYSREEIL  422
AtFKF1-LOV   (aa 28-174)    28: NDGIEDQVEDEKLPLEVGMFVYPWTPPSFIVSDALEPDFPLIYVNRVFEVFTGYRADEVL   87
AtLKP2-LOV   (aa 19-164)    19: VAEDGWFGGDNGAIPFPVGSLPGTAPCGFVVSDALEPDNPIIYVNTVFEIVTGYRAEEVI   78
AtZTL-LOV    (aa 19-165)    19: DDEEGGLFPGGGPIPYPVGNLLHTAPCGFVVIDAVEPDQPIIYVNTVFEMVTGYRAEEVL   78
                                  .   .   . .   *...*.  *. *.....  *  *.* .*..

                                                                    ☆
231: GMMCRFLQGSG----------IDADELAKIRETLAAGMNYCGRILNYKKDGTSFWNLLTIAPIKDESGEVLKFIGMQVEVSKHTEGAK  308
509: GMMCRFLQGPE----------TDLTTVEKIRNAINQTEVTVQLINYTKSGKKFWNIFHLQPMRDQKGEVQYFIGVQLDGSEHVEPVR  586
167: GMMCRFLQGPD----------TDKNEVAKIRDCVENGKSVCGRLLNYKKDGTPFWNLLTVTPIKDDQGNTIKFIGMQVEVSKYTEGVN  244
423: GMMCRFLQGPE----------TDQATVQKIRDAIDQREITVQLINYTKSGKKFWNLFHLQPMRDQKGELQYFIGVQLDGSDHVEPLQ  500
 88: GRMCRFLQYRDPRAQREHPLVDPVVVSEIRRCLEEGIEFQGELLNFRKDGTPLVNKLRLAPIRDDDGTITHYIGIQVFSETTIDLDR  174
 79: GMMCRFLQCRGPFTKRRHPMVDSTIVAKMRQCLENGIEFQGELLNFRKDGSPLWNKLRLVPIREEDE-ITHFIGVLLFTDAKIDLGP  164
 79: GGMCRFLQCRGPFAKRRHPLVDSMVVSEIRKCIDEGIEFQGELLNFRKDGSPLWNRLRLTPIYGDDDTITHIIGIQFFIETDIDLGP  165
     *.******.          . .*   . ..*. .  . .  . .**. *.* ***.* . . *.**.  .    .** .  .   .
```

b.

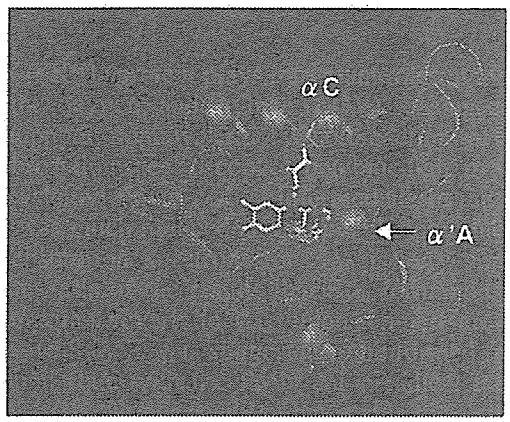

FIGURE 1: (a) Multiple sequence alignment of phototropin and FKF1-type LOV domains in *A. thaliana*. LOV sequences in the alignment include the following: *A. thaliana* phot1 (AAC01753) and phot2 (AAC27293), FKF1 (AF216523), LKP2 (NP849983), and ZTL (AF252294). Asterisks indicate 100% identity, and dots indicate similarity. The LOV core region (*40*) and the conserved cysteine for FMN binding are indicated by arrows and a star, respectively. FKF1 is shown by pink letters, in which a nine amino acid insertion characteristic with the FKF1-type LOV is shown by green letters. The indicated amino acid sequence of FKF1 (Asp28−Arg174) is used in this experiment. (b) Cartoon modeling of the predicted three-dimensional (3D) structure of the FKF1-LOV core domain. 3D structure prediction for the FKF1-LOV was carried out using an automated comparative protein-modeling server, Swiss Model (http://swissmodel.expasy.org/). The nine amino acid insertion between the α′A-helix and αC-helix (helical connector) and the conserved photoactive cysteine are colored by green and yellow, respectively. FMN is shown by stick modeling. Carbon, nitrogen, oxygen, and phosphorus atoms in the FMN molecule are colored by white, blue, red, and orange, respectively.

the binding is thought to be controlled by light received by the LOV domain.

Photoreactions of the LOV domains in phot have been well established. Upon absorbing blue light, the LOV domains undergo a unique photochemical reaction cycle. The ground state of the FMN in the LOV domains shows typical absorption spectra of flavoproteins with an absorption maximum from 445 to 450 nm and named D_{450}, that is excited to a singlet excited state by blue light and then interconverted to a triplet excited state, L_{660} (*28*). FMN in the L_{660} forms an adduct with a nearby cysteine conserved in all of the LOV domains with a time constant of ca. 4 μs, that has an absorption maximum from 380 to 390 nm and is termed S_{390} (*28*−*30*). Recently, a new photointermediate state was detected that has the same electronic structure around the FMN chromophore, however, a different protein structure from those of the S_{390} (*30*−*33*), and is thought to be a signaling state. To discriminate the two S_{390}, we have proposed recently to name them as S_{390}I and S_{390}II (*34*). S_{390} reverts to D_{450} with time constants from several seconds to a few minutes depending on the species (*35*).

In contrast to the LOV domains of phot, photoreactions of the LOV domains in FKF1 families have been poorly understood. They form a photointermediate state alike to the S_{390} that are reported to be not reversible to D_{450} after 40 min (*17*) or 2 h (*36*). LOV domains of the FKF1 families have a nine amino acid insertion between the α′(A)-helix having the conserved cysteine and α(C)-helix (helical connector) as compared to those of phot families (Figure 1). The observed irreversibility may come from this structural difference and possibly be correlated with the different functions between them. Phot has Ser/Thr kinase in the C-terminal region, and the LOV domains act as a light-regulated molecular switch of the kinase in both in vivo autophosphorylation (*37*) and in vitro substrate phosphorylation (*38*). On the other hand, LOV domains of FKF1 families are involved in the formation of protein complexes, for example, FKF1 with CDF1(*24*), ZTL with TOC1 (*12*), and LKP2 with PRR1(TOC1) and PRR5 (*39*).

To understand the molecular bases underlying the different functions between the phot-type and the FKF1-type LOV domains, it is requisite to establish the photoreaction of the FKF1-type LOV domain. We, therefore, investigated the photoreaction of the LOV domain of FKF1 by low-temperature UV−visible absorption spectra and figured out the photoreaction including a novel photoproduct at low temperature. Furthermore, we found that the S_{390} of the FKF1-LOV also reverts to D_{450} at room temperature although its reversion is very slow. The photoreaction kinetics is

discussed on the basis of these data, together with the calculated activation energies of the reactions.

MATERIALS AND METHODS

Preparation of Recombinant LOV-Containing Polypeptide. A LOV domain-containing polypeptide of *A. thaliana* FKF1 protein was prepared by an overexpression system with *Escherichia coli* (*E. coli*). Using *Arabidopsis* cDNA as a template, a DNA fragment corresponding to the polypeptide from Asp28 to Arg174 was amplified by the PCR method with primers providing appropriate restriction sites. That has 26 and 8 extra amino acid sequences to the N- and C-termini, respectively, of the LOV core (*40*). The amplified DNA was isolated, digested, and cloned into a pGEX4T1 expression vector (Amersham Biosience) as a fusion protein with glutathione *S*-transferase (GST). Its nucleic acid sequences were verified by DNA sequencing with a CEQ2000XL DNA analysis system (Beckman Coulter). *E. coli* JM109 strain transformed by the expression vector was grown at 310 K in LB medium containing 50 μg mL^{-1} ampicillin until A_{600} comes to 0.3 and then incubated with 0.1 mM isopropyl β-D-thiogalactopyranoside for 20 h at 293 K in darkness. The following purification procedures were carried out at 273–277 K under dim red light. Bacteria were collected by centrifugation, washed with phosphate-buffered saline (PBS, 8.0 mM Na_2HPO_4, 1.5 mM KH_2PO_4, 140 mM NaCl, and 2.7 mM KCl, pH 7.4), and resuspended in PBS containing 1 mM phenylmethanesulfonyl fluoride (PMSF). The cells were lysed by sonication, and the supernatant was mixed with glutathione–Sepharose 4B (Amersham Bioscience). After the resin was washed with PBS, the LOV polypeptides were cleaved from the GST tag with thrombin that leaves two extra amino acid residues, Gly-Ser, to the N-terminus of the LOV-containing polypeptide. The dissociated polypeptides from the gel were purified further by gel filtration on a Sephacryl S-100 HR column (Amersham Bioscience) equilibrated and eluted with 100 mM NaCl, 25 mM Tris-HCl, and 1 mM Na_2EDTA (TBS, pH 7.8). The purity of the polypeptides was examined with Coomassie Blue staining of SDS–PAGE.

UV–Visible Absorption Spectra Measurement of the Solution Sample at Room Temperature. The purified FKF1-LOV polypeptide in TBS was concentrated to give a final concentration with λ_{450} = 0.4 using a Microcon YM-10 instrument (Millipore) at 277 K. Reversion from S_{390} to D_{450} of the polypeptide solutions in the dark was monitored with a UV-3310 spectrophotometer (Hitachi) at room temperature, 298 K. Blue light was supplied with a combination of a 1 kW projector (OLYMPUS) and a plastic filter sheet (λ_{max} of 480 nm and half-width of 40 nm; Nakagawa Chemicals) to activate the solution sample.

UV–Visible Absorption Spectra Measurement of the Hydrated Film Sample at Low Temperature. The purified FKF1-LOV polypeptide in TBS was concentrated to give a final concentration with λ_{450} = 1.5 using a Microcon YM-10 instrument (Millipore) and then dialyzed against 1 mM potassium phosphate (pH 7.0) at 277 K. Hydrated films were prepared after the procedure described before (*30*). Briefly, 70–80 μL of the solution was placed on a BaF2 window and then dried under reduced pressure. Dried films were hydrated by dropping H_2O next to the film on the plate and sealing it with one more plate and a silicon rubber gasket. UV–visible absorption spectra of the films were measured using V-550DS (JASCO) spectrophotometers. To measure low-temperature spectra, a cryostat (Optistat DN, Oxford) and a temperature controller (ITC 4, Oxford) were used with liquid nitrogen as coolant. The spectra were measured at eight different temperatures in which a new sample was used at each temperature. As a light source for activating the film samples, a combination of a 1 kW halogen–tungsten lamp and a long-pass filter (L42, Asahi Techno Glass) were used that gives a >400 nm light. In case to attenuate the light intensity, a 25% neutral density filter (ND-25, Asahi Techno Glass) was used.

RESULTS

Blue Light-Induced UV–Visible Absorption Spectral Changes in Hydrated Films Measured at 77–298 K. Blue light induced UV–visible absorption spectral changes of the FKF1-LOV containing polypeptide were measured at eight different temperatures, 298, 250, 200, 175, 150, 125, 100, and 77 K. Six of them are presented in the Figure 2. At 298 K, the polypeptide in the hydrated films prepared in the dark showed a typical spectrum of flavin in a protein pocket with λ_{max} at 450 nm (Figure 2a, 298 K, black line). Here, we call the dark state as D_{450} after the nomenclature of phot in the photocycle. The triplet peak bleached, and a new major peak and a broad shoulder appeared at 378 nm and in 300–320 nm, respectively, upon blue light irradiation (Figure 2a, 298 K, from green to brown lines). The absorption spectrum of this photointermediate state (Figure 2, 298 K, red line) is similar to those of S_{390} of oat phot1 LOV2 with λ_{max} at 390 (*28*) or 380 (*41*) nm, that we also name as S_{390}. At 250 (data not shown) and 200 K (Figure 2a, 200 K), similar light-induced absorption spectral changes were observed although prolonged irradiation is required in the latter case. At 175 K, however, even irradiation for 1 h could not complete S_{390} formation (data not shown) that showed spectral changes similar to those at 150 K (Figure 2a, 150 K). At 125 K, a new peak appeared at 370 nm as well as S_{390} formation (Figure 2a, 125 K) after 1 h irradiation, in which D_{450} bleaching was much reduced. The new peak became more prominent according with the decrease of the temperature. At 77 K, S_{390} formation almost disappeared and only the formation of the new species with λ_{max} at 370 nm was detected, which we propose to name Z_{370}. Formation of Z_{370} did not accompany the appearance of the shoulder at 300–320 nm observed with S_{390} formation (Figure 2a, 77 K).

Light minus dark absorption difference spectra revealed increased formation of Z_{370} at lower temperatures more clearly (Figure 2b). The S_{390} minus D_{450} spectrum obtained at 298 K has characteristic negative peaks at 370 and 450 nm and positive peaks at 310 and 390 nm, respectively. On the other hand, light minus dark spectra below 200 K showed an appearance of a peak at 370 nm that became recognizable as a positive peak at 150 K, comparable with the peak of S_{390} at 390 nm at 125 K, and dominant at 77 K. These results clearly show the formation of a novel photoproduct, Z_{370}, at the low temperatures.

Dependence of S_{390} and Z_{370} Formation on the Blue Light Irradiation Time at 150 K in Hydrated Films. The time course of the blue light-induced S_{390} and Z_{370} formation at

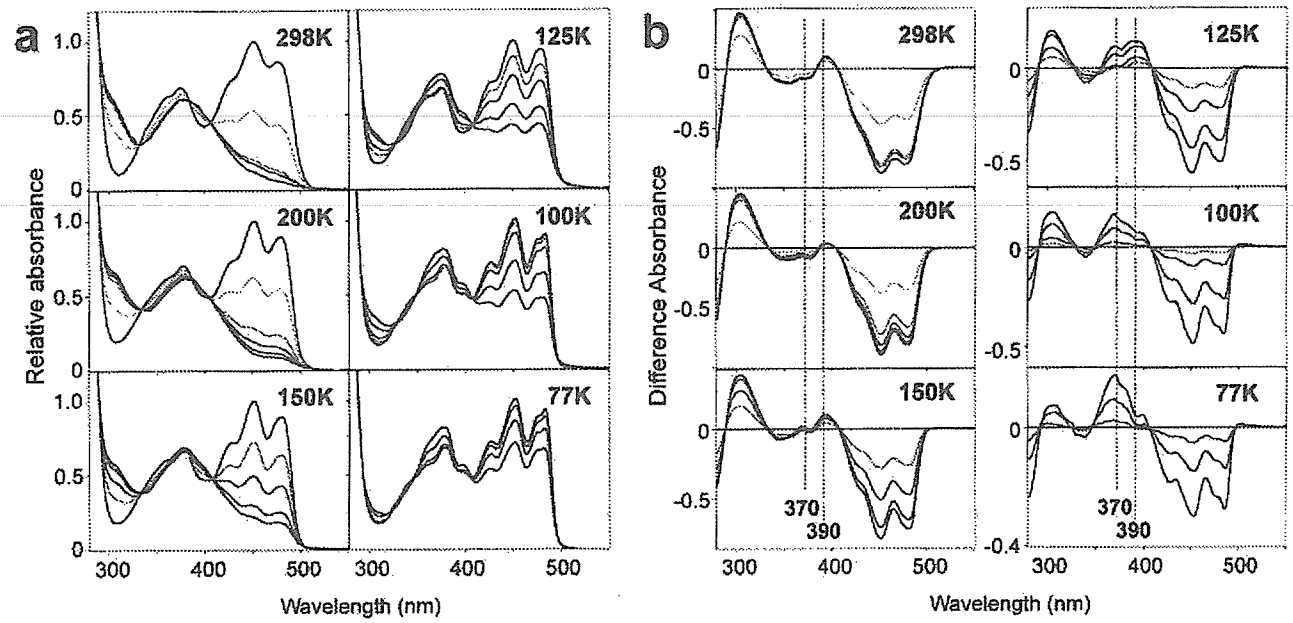

FIGURE 2: Blue light-induced absorption (a) and light-minus-dark absorption difference (b) spectra changes of *Arabidopsis* FKF1-LOV-containing polypeptide in a hydrate film measured at eight different temperatures from 298 to 77 K, where six results are presented with the measured temperatures. Irradiation times are 0 s (black), 2 s (yellow), 10 s (green), 1 min (blue), 10 min (purple), and 60 min (red).

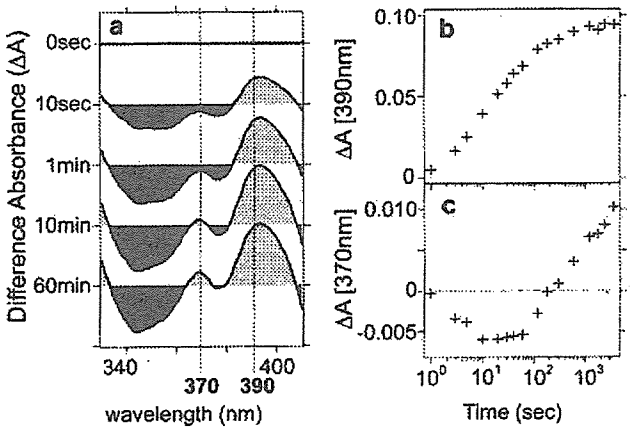

FIGURE 3: Blue light-induced light-minus-dark absorption difference spectra changes of *Arabidopsis* FKF1-LOV-containing polypeptide in a hydrate film measured at 150 K in the wavelength region from 330 to 410 nm (a) adapted from the spectra in Figure 2. Positive and negative areas are colored with light gray and dark gray, respectively. Time courses of the blue light-induced light-minus-dark absorption difference at 390 (b) and 370 (c) nm, where the time scale is logarithmic.

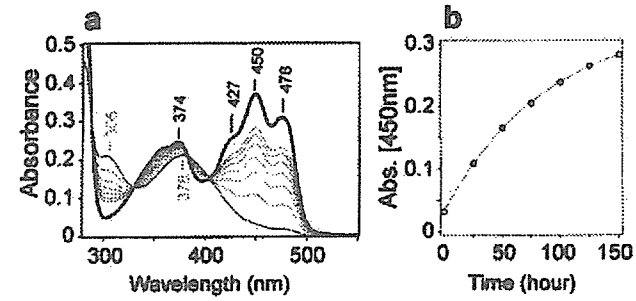

FIGURE 4: Absorption spectra of *Arabidopsis* FKF1-LOV-containing polypeptide in a 100 mM NaCl, 25 mM Tris-HCl, and 1 mM Na_2EDTA (pH 7.8) solution at 298 K before 1 min blue light irradiation (black) and immediately and every other 25 h after the irradiation (gray) (a) and the time course of absorption change at 450 nm (b) where the fitting curve was calculated by a method of nonlinear least squares.

150 K was analyzed using the data presented in Figure 2b. The absorption difference spectra in the wavelength region from 330 to 410 nm are magnified to trace the S_{390} and Z_{370} formation (Figure 3a). The absorbance increase at 390 nm representing S_{390} formation is almost in proportion to logarithmic irradiation time until 100 s and then gradually saturated (Figure 3b). On the other hand, the absorbance change at 370 nm showed a decrease until 20 s and then a linear increase until 60 min (Figure 3c). Since absorption at 370 nm decreases by S_{390} formation, the transient absorption decrease at 370 nm indicates delayed formation of Z_{370} to that of S_{390}. The delayed formation of Z_{370} to S_{390} formation excludes the possibility that Z_{370} is an intermediate between D_{450} and S_{390}. On the contrary, the delay raises the possibility that a part of S_{390} is photoconvertible to Z_{370} by prolonged irradiation of blue light as well as a simple interpretation that Z_{370} formation is delayed to S_{390} formation. However, the possibility can be excluded since Z_{370} formation decreased according to the temperature increase and disappeared at 298 K.

Reversion of S_{390} to D_{450} in the Dark in Solution at 298 K. S_{390} of the FKF1-LOV domain is reported not to revert to D_{450} in the dark; however, we found accidentally that S_{390} of our FKF1-LOV-containing polypeptide does revert to D_{450}. Then, the time course of the reversion was measured at room temperature, 298 K, in the TBS solution. Reverted spectra exhibited a vibrational structure in the main peak region (427, 450, and 478 nm) identical to that of D_{450} (Figure 4a). The time course of the reversion monitored at the absorption increase at 450 nm can be well simulated by a single exponential curve with a half-life time of 62.5 h (Figure 4b). These results indicate that S_{390} reverts to D_{450} through thermal processes very slowly at room temperature.

Calculation of an Absolute Absorption Spectrum of Z_{370} in Hydrated Films. An absolute absorption spectrum of Z_{370} was obtained by calculation from that in the photostationary state among Z_{370}, S_{390}, and D_{450} at 100 K, in which the other

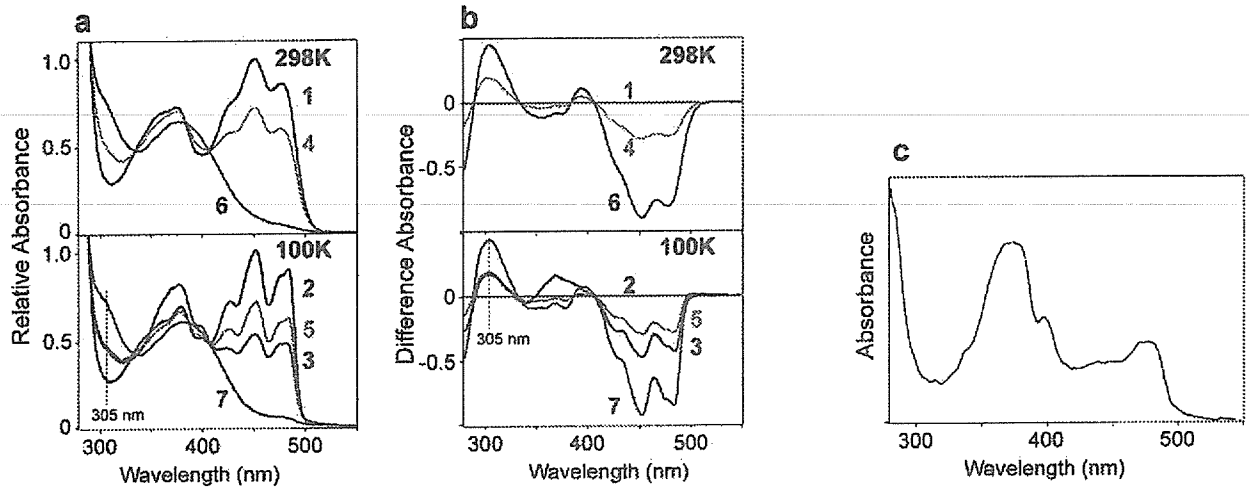

FIGURE 5: Absorption spectra (a) and light-minus-dark absorption difference spectra (b) changes of *Arabidopsis* FKF1-LOV-containing polypeptide in a hydrate film to calculate an absorption spectrum for Z_{370} (c). Absorption spectra were measured at either 298 K (upper) or 100 K (lower). The order of the measurements is indicated by the numbers attached to each spectrum. For details of the measurements, see the Results section.

populations can be negligible. At first, an absorption spectrum of D_{450} at 100 K was obtained that showed a more pronounced vibrational structure (Figure 5a, 2, 100 K) than that at 298 K (Figure 5a, 1, 298 K). One hour blue light irradiation at 100 K produced Z_{370} as well as S_{390} (Figure 5a, 3, 100 K) as described above. To obtain the absorption spectrum of S_{390}, the sample was then heated to 298 K (Figure 5a, 4, 298 K). Interestingly, the absorption peak at 370 nm disappeared, suggesting the thermal conversion of Z_{370} to D_{450} upon heating to 298 K. To verify this, the sample was again cooled to 100 K (Figure 5a, 5, 100 K). Comparison of the two spectra at 100 K between before and after the heating to 298 K revealed a marked decrease of the absorption around 370 nm and an increase in the main peak region of D_{450}, supporting the interpretation that Z_{370} was converted to D_{450} thermally upon heating. Next, the sample was heated to 298 K and then irradiated with blue light for 5 min that converted the sample completely to S_{390} (Figure 5a, 6, 298 K). Then the sample was cooled dawn to 100 K again and an absorption spectrum of S_{390} at 100 K was obtained (Figure 5a, 7, 100 K).

On assumption that the observed spectra at 100 K consist of the three spectra for D_{450}, S_{390}, and Z_{370} and that the reversion of S_{390} to D_{450} is negligible in this time range (Figure 4b), the absorption spectrum of Z_{370} was calculated using the following three spectra, where A and B are the photoconverted fraction of D_{450} to S_{390} and Z_{370}, respectively: D_{450} (Figure 5a, 2); $(1 - A - B)D_{450} + AS_{390} + BZ_{370}$ (Figure 5a, 3); $(1 - B)D_{450} + AS_{390}$ (Figure 5a, 5).

The spectrum of (Figure 5a, 2) minus (Figure 5a, 3) plus B(Figure 5a, 2) gives the spectrum of BZ_{370}. The spectrum of Z_{370} (Figure 5c) was obtained by dividing this spectrum by B that was determined to be 0.35 so as to cancel the negative main peaks of D_{450}. The spectrum has a major and a minor peak at 370 and 400 nm, and a broad peak at 460–480 nm, respectively. They are characteristic with the flavoproteins in the anion radical states (*42–46*). For example, the present spectrum is very similar to those in Figure 6, dashed line of ref *43*, or Figure 4A of ref *44*, although absorption peaks of our spectrum are much narrower and have less tailing due to sharpening at low temperature.

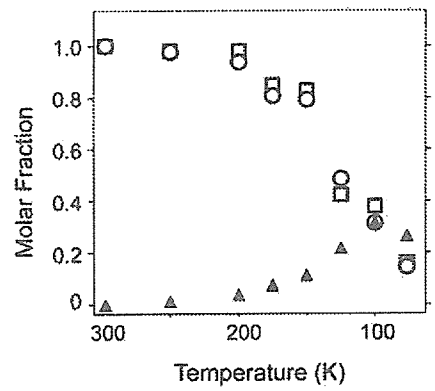

FIGURE 6: Molar fraction of D_{450} converted to S_{390} or Z_{370} by 1 h blue light irradiation at 298–77 K in hydrated films of *Arabidopsis* FKF1-LOV-containing polypeptide. (○), (□), and (△) represent the S_{390} fractions determined by cool-heating cyclic measurements at 450 nm, S_{390} fractions determined at 305 nm, and Z_{370} fractions. For calculation of the molar fraction, see the Results section.

The absorption spectrum of a film irradiated with blue light at 100 K, heated to 298 K, and then cooled and measured at 100 K minus that of D_{450} at 100 K has a shape similar to that of 100% S_{390} minus D_{450} measured at 100 K. This indicates that Z_{370} produced at 100 K by blue light was completely returned to D_{450} by the heating to 298 K.

Fraction of S_{390} and Z_{370} Formed in Hydrated Films at Different Temperatures. To determine the molar fraction of FKF1-LOV-containing polypeptide converted to S_{390}, the same cool-down and heat-up cycling measurements as shown in Figure 5 were performed at seven different temperatures as well as the measurement at 298 K. Molar fractions converted to S_{390} by 1 h blue light irradiation at temperature t, $F(t)$, is expressed as

$$F(t) = [\mathrm{At}(1) - \mathrm{At}(4)]/[\mathrm{At}(1) - \mathrm{At}(6)]$$

where At(1), At(4), and At(6) are the absorption at 450 nm of the spectra corresponding to 1, 4, and 6 of Figure 5a at temperature t. Calculated molar fractions are plotted against temperature (Figure 6, circle). At 298–200 K, D_{450} was almost completely phototransformed to S_{390}; however, the photoconvertible fraction decreased with the decrease of

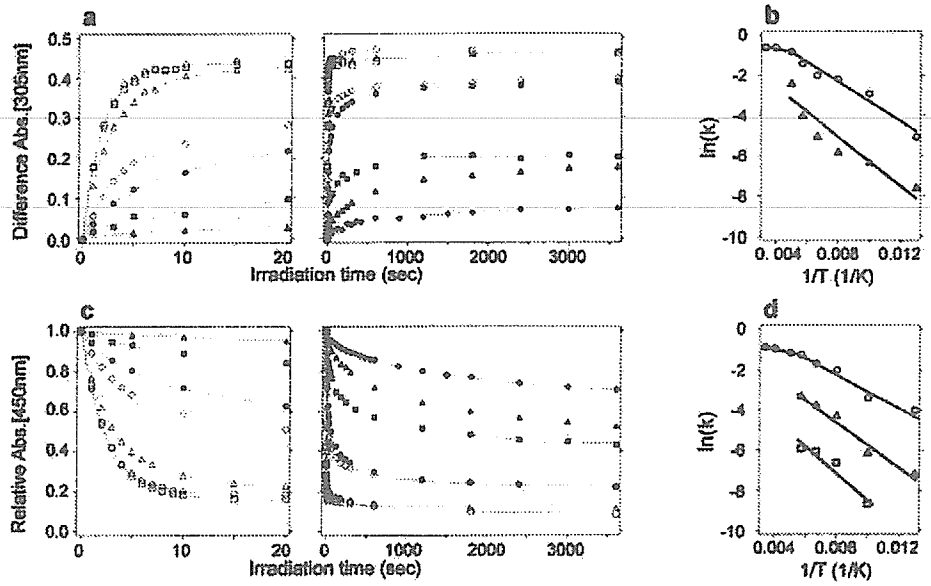

FIGURE 7: Time courses of blue light-induced absorption difference change at 305 nm (a), and absorption change at 450 nm (b), until 20 s (left) and 60 min (right) at 298 K (○), 250 K (□), 200 K (△), 175 K (◇), 150 K (●), 125 K (■), 100 K (▲), and 75 K (◆) of hydrated films of *Arabidopsis* FKF1-LOV-containing polypeptide. Fitting curves are obtained by a method of nonlinear least squares. For details of the fitting conditions, see the text. Arrhenius plots of the rate constants obtained from the time course shown in (a), (c) and in (b), (d). The straight lines were calculated by the method of least squares.

temperature below 200 K. At the liquid nitrogen temperature, only 15% was converted to S_{390}, that may be explained by either the increased population that cannot be converted to S_{390} or a decreased rate of the reaction at the low temperatures. The former possibility was discussed in LOV2 of *Adiantum* phytochrome3 (phy3) (*47*, *48*) on the basis of an unfavorable molecular position of the SH group to FMN to form a cysteinyl-flavin adduct revealed in the crystal structure of *Chlamydomonus* phot-LOV1 (*49*).

In addition to the absorption at 450 nm, that at 305 nm can be used to estimate the amount of S_{390} formed. As can be seen from the comparison of the absorption spectra in Figure 5a,b, the absorption at 305 nm of D_{450} was little affected by the presence of Z_{370}. The absorption change at 305 nm, thus, represents only S_{390} formation. Using this absorption, S_{390} formation can be quantified without the cool-down and heat-up cycling measurements. The result is indicated also in Figure 6 (box) that well coincides with the temperature-dependent curve determined by the absorption at 450 nm (circle). Together with the absorption spectrum of Z_{370} (Figure 5c), this confirms the absorption at 305 nm to be a good indicator for S_{390} formation.

Molar factions of Z_{370} formed by blue light irradiation were determined as follows. In comparison of the D_{450} spectrum of a film with its 100% S_{390} form, the relation, $A(450) = 1 - 0.90X$, was obtained where $A(450)$ is the absorption at 450 nm of a film after a molar fraction, X, is converted from D_{450} to S_{390}. By comparing the absorption spectra of D_{450} and Z_{370} normalized to the absorption at 305 nm based on the observation described above, the relation, $A(450) = 1 - 0.61Y$ was obtained, where $A(450)$ is the absorption at 450 nm of a film after a molar fraction, Y, is converted from D_{450} to Z_{370}. In combination of the two relations, $A(450)$ can be expressed as $1 - 0.90X - 0.61Y$. Y was calculated from the equation using the X determined by $A(450)$ in the previous section (Figure 6, circle) and shown also in Figure 6 (triangle). Z_{370} was formed below 200 K and increased according to the decrease of temperature until 100 K. At 77 K, in turn, it decreased.

Calculation of the Activation Energy for Photoreaction from D_{450} to S_{390} or Z_{370}. To calculate the activation energy of the photoreaction from D_{450} to S_{390}, the time course of the blue light-induced reaction was monitored by the absorption change at 305 nm as described in the previous section. The absorption changes are well simulated by a single exponential curve above 200 K and biexponential curves from 200 K to liquid nitrogen temperature (Figure 7a). An Arrhenius plot of the rate constants (Figure 7b) revealed an activation energy of 1.2 kJ/mol with the single component above 200 K and 3.8 and 4.8 kJ/mol with the two components below 200 K, respectively, indicating the presence of two different pathways from D_{450} to S_{390} at the lower temperatures. Furthermore, a discontinuity at 200 K in the first component suggests some conformational changes of the LOV polypeptide around 200 K.

Photoreaction kinetics was also monitored at 450 nm that reflects the photoactivation of D_{450}. In contrast to those at 305 nm, the changes are well simulated by a single exponential curve above 175 K and triexponential curves from 175 K to liquid nitrogen temperature (Figure 7c). An Arrhenius plot of the rate constants (Figure 7d) gave an activation energy of 1.4 kJ/mol for the single component above 175 K that well agrees with the 1.2 kJ/mol obtained from 305 nm change although the temperature ranges differ slightly. The plot also showed 3.3, 4.7, and 5.4 kJ/mol for the three components, respectively. The activation energy of the former two, 3.8 and 4.8 kJ/mol, well correspond to those observed with S_{390} formation detected by the 305 nm change, suggesting that the two come from S_{390} formation. The third component with 5.4 kJ/mol, therefore, may be attributable to formation of Z_{370}. The populations of the three components were also calculated (data not shown). The first component decreased almost linearly with the decrease of temperature, whereas the second component showed a

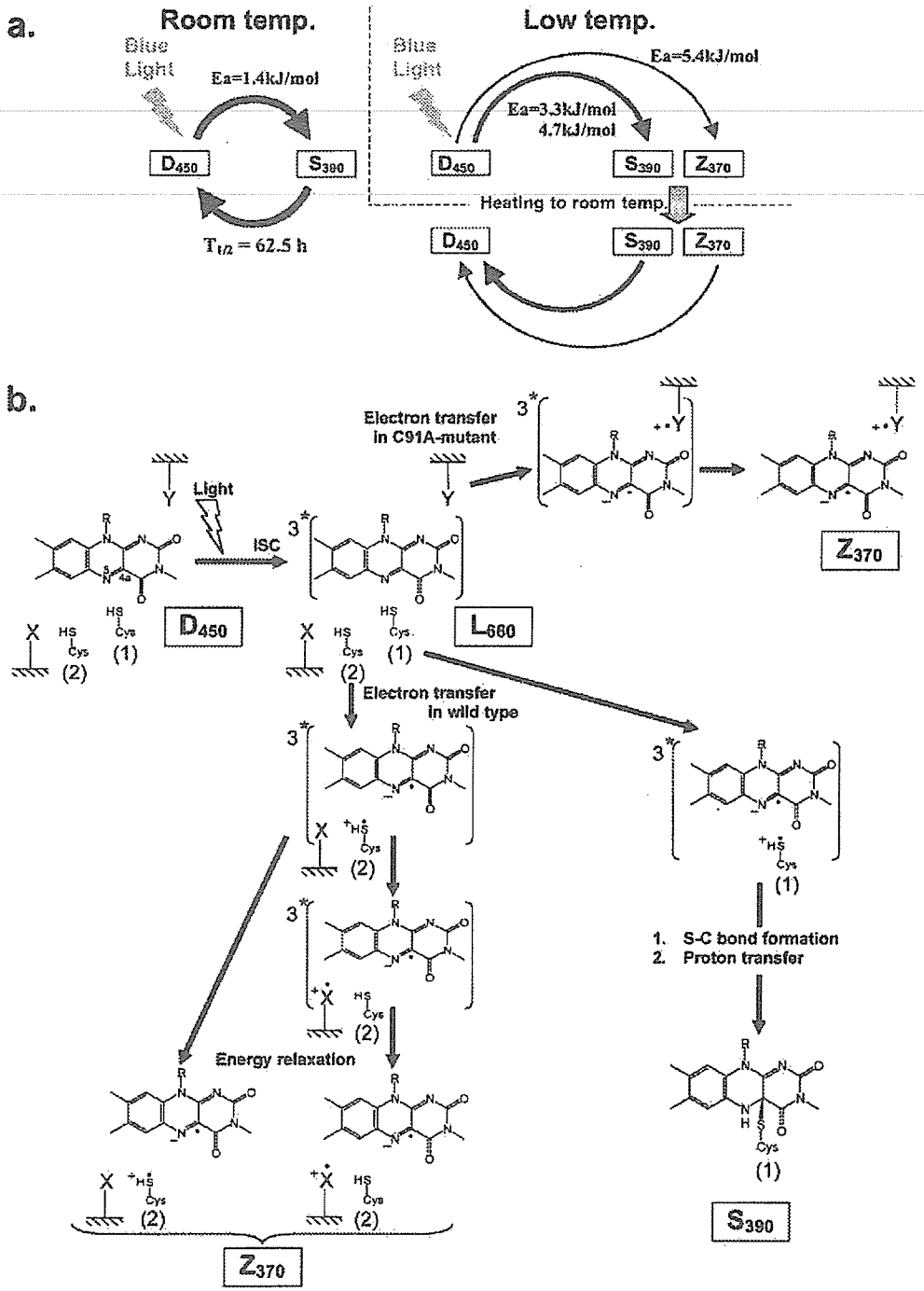

FIGURE 8: (a) Summary of the photoreaction cycle of the LOV-containing polypeptide of *Arabidopsis* FKF1. (b) Possible reaction pathways for Z_{370} formation at low temperature in the LOV-containing polypeptide of *Arabidopsis* FKF1. The upper right part is that for the C91A mutant of the polypeptide; the other part is for the wild-type polypeptide. (1) and (2) represent the SH group of the conserved cysteine in a right or a wrong position to form a cysteinyl-flavin adduct. 3* indicates the triplet-excited state. X and Y represent unidentified amino acid residues involved in the electron transfer reactions. X and Y cannot be distinguished at this moment. For details, see the Discussion.

maximum population around 200 K. The third component increased below 200 K that well agrees with the increased molar fraction of Z_{370} below 200 K (Figure 6, triangle), supporting the assignment of this component to Z_{370}.

DISCUSSION

Reversion of S_{390} to D_{450}. LOV domains of FKF1 families form a stable photointermediate state alike to S_{390} of phot. The S_{390} cannot be produced upon introduction of the mutation into the conserved cysteine (*17*), suggesting a cysteinyl-flavin adduct formation similar to that in S_{390} of phot (*28*–*30*, *50*, *51*). This S_{390} of FKF1 families has been thought to be irreversible to the ground state. In this study, we demonstrated clearly the reversion of S_{390} to D_{450} with a half-life time of 62.5 h (Figure 4). This is summarized in Figure 8a, left. This extremely slow reversion may derive from the nine amino acid insertion to the LOV core amino acid sequence of phot (Figure 1a). The insertion resides between the α′A-helix and αC-helix (helical connector). The former possesses the conserved photoactive cysteine, and the latter interacts with the ribitol and the phosphate groups of FMN (*47*, *49*) (Figure 1b). The NMR spectrum of the

phosphate group has been reported to change upon photoactivation (*52*). Since both of the helices are deeply involved in the photoreaction of phot LOV, the nine amino acid insertion could modify the dark reversion of FKF1-type LOV domains (Zikihara et al., manuscript in preparation). The slow reversion of LOV domains of FKF1 may have some role in its function, such as light-regulated formation of a stable protein complex that contributes to proper ubiquitination of target proteins.

In phot, the reversion takes place with the half-life times from several seconds to a few minutes at ambient temperatures (*35*). At the low temperatures where S_{390} is stable, a photoconvertible fraction of D_{450} to S_{390} becomes smaller. These make the spectroscopic or structural studies on S_{390} difficult in phot families. In contrast, S_{390} of FKF1-LOV is very stable and can serve as an useful sample for these kinds of studies, especially for crystallization of LOV domains in a real S_{390} state. The LOV domain of FKF1 families has no tryptophan in contrast to the presence of one tryptophan in phot LOV. This makes the light-induced spectral changes in the UV region clearer. Actually, the absorption spectrum of S_{390} of FKF1-LOV showed a minor peak at 305 nm as well as a main peak at 378 nm, which is not seen in the spectrum of phot LOV due to large absorption of the tryptophan overlapping the absorption of FMN in this region. Accordingly, FKF1-LOV is a good sample to study the photointermediate states of LOV domains.

A Novel Photoproduct Z_{370}. The present low-temperature spectroscopic study detected a new photoproduct, Z_{370}, that appears below 200 K and dominated at liquid nitrogen temperature. The possibility that Z_{370} is an intermediate from D_{450} to S_{390} trapped at low temperature can be excluded on the basis of the following evidence. First, if so, molar factions of S_{390} produced at low temperatures will increase upon heating due to the conversion of Z_{370} to S_{390}. However, the population of S_{390} did not increase; instead, Z_{370} reverted to D_{450} (Figure 5a,b and Figure 8a, right). Second, evidence indicates that S_{390} formation proceeds Z_{370} formation (Figure 3). Then, a question arises, what does Z_{370} come from? FMN in Z_{370} is very likely to be an anion radical state judging from its absorption spectrum as mentioned in the Results. It has been proposed that a radical pair is formed between FMN and cysteine in the triplet state that makes FMN an anion radical (state C, in Figure 7 of ref *41*). Therefore, Z_{370} is suggested to be formed from this biradical triplet excited state after relaxing to the ground state with the FMN anion radical trapped at the low temperature. For the fate of the counter SH cation radical, there may be two possibilities. The SH cation radical may also be trapped at the ground state in case that the distance between the radical pair is enough to prevent the back-electron transfer. The second possibility is that the cation radical accepts an electron from an unidentified redox-active amino acid residue to revert to the ground state. Since the C91A mutant of the FKF1-LOV domain also showed formation of Z_{370} at 77 K (data not shown) indicating the presence of a redox-active amino acid residue other than the cysteine near the FMN isoalloxazine ring, the second case is very probable. Similar electron transfer from the other amino acid than the cysteine has been reported with the oat phot1 LOV2 C450A mutant (*50*). EPR study on Z_{370} will clear these points. These schemes are illustrated schematically in Figure 8b.

A probable origin for Z_{370} formation is discussed below. The photoconverted fraction of D_{450} to S_{390} decreased according to the temperature decrease (Figure 6). Similar decreases in the photoconvertible population at low temperatures were reported with *Adiantum* phy3-LOV2 (*30*, *54*) and suggested to derive from fixation of an unfavorable SH position relative to FMN to form a cysteinyl-flavin adduct at lower temperatures. Actually, the crystal structure of *Chlamydomonus* phot-LOV1 has revealed the presence of two, the right and the wrong, SH positions (*49*). Accordingly, the SH in the wrong position that is able to produce a radical pair but unable to form the adduct may originate Z_{370}. A slightly different molecular structure of FKF1-LOV from those of phot-LOV possibly due to the nine amino acid insertion etc. may enable the formation of this particular molecular species. The situation is also illustrated in Figure 8b. This scheme supports the proposal that electron migration proceeds proton transfer from the photoreactive cysteine to C(4a) of the FMN isoalloxazine ring (*41*).

It has been proposed that only a zwiterionic intermediate adduct without proton transfer (state D in Figure 7 of ref *41*) is formed at 80 K but S_{390} is not in oat phot1-LOV2. However, the red-shifted species corresponding to this state was undetectable in the FKF1-LOV samples at 77 K. Low-temperature FTIR and UV−visible spectra studies on *Adiantum* phy3-LOV have shown deprotonation of the SH and S_{390} formation at 77 K, that is marked in LOV2 but obscure in LOV1 (*30*, *51*, *53*). In FKF1-LOV, S_{390} formation was also observed at 77 K.

Activation Energy of the Photoreactions. The activation energy of S_{390} formation was calculated to be 1.4 kJ/mol above 200 K and 3.3 and 4.7 kJ/mol below 200 K, indicating a discontinuity around 200 K. Recently, the activation energy of S_{390} formation in *Adiantum* phy3-LOV2 was reported to be 0.67 and 1.04 kJ/mol below 200 K (*54*) that are comparable, however somewhat smaller than those of FKF1-LOV. In phy3-LOV2, blue light irradiation for a few minutes converted 64% and 36% of D_{450} to S_{390} at 100 and 77 K, respectively (*30*, *53*, *54*), while 1 h irradiation induced only 35% and 15% photoconversion to S_{390} at 100 and 77 K, respectively, in FKF1-LOV (Figure 6). These suggest lower quantum efficiency of the photoreaction in FKF1-LOV and may explain the larger activation energy in FKF1-LOV.

The activation energy of Z_{370} formation was calculated to be 5.4 kJ/mol that is larger than those of S_{390}, although the reaction may not include proton migration since SH of the cysteine is reported to be protonated in the triplet excited state (*55*). The larger activation energy may partly come from the larger energy barrier of electron migration from the wrong SH position than that of the right position.

Concluding Remarks. Cyclic photoreaction of the FKF1-LOV domain is established by the present study that includes a different pathway from S_{390} formation (Figure 8). The photoreaction cycle together with the activation energy provided useful information to figure out the molecular mechanism underlying the photoreaction of FKF1-LOV. To understand more precisely the photoreaction mechanism, the role of the nine amino acid insertion is under investigation.

ACKNOWLEDGMENT

The authors thank Dr. S. Yoshihara and Ms. S. Konishi at K.Z. and S.T.'s Laboratory for stimulating discussion and technical assistance, respectively, and Dr. T. E. Swartz at the Department of Chemistry and Biochemistry, University of California, Santa Cruz, for valuable advice for the protein modeling.

REFERENCES

1. Christie, J. M., and Briggs, W. R. (2001) Blue light sensing in higher plants, *J. Biol. Chem. 276*, 11457−11460.
2. Celaya, R. B., and Liscum, E. (2005) Phototropins and associated signaling: providing the power of movement in higher plants, *Photochem. Photobiol. 81*, 73−80.
3. Liscum, E., and Briggs, W. R. (1995) Mutations in the *NPH1* locus of *Arabidopsis* disrupt the perception of phototropic stimuli, *Plant Cell 7*, 473−485.
4. Kagawa, T., Sakai, T., Suetsugu, N., Oikawa, K., Ishiguro, S., Kato, T., Tabata, S., Okada, K., and Wada, M. (2001) *Arabidopsis* NPL1: a phototropin homolog controlling the chloroplast high-light avoidance response, *Science 291*, 2138−2141.
5. Jarillo, J. A., Gabrys, H., Capel, J., Alonso, J. M., Ecker, J. R., and Cashmore, A. R. (2001) Phototropin-related NPL1 controls chloroplast relocalization induced by blue light, *Nature 410*, 952−954.
6. Kinoshita, T., Doi, M., Suetsugu, N., Kagawa, T., Wada, M., and Shimazaki, K. (2001) phot1 and phot2 mediate blue light regulation of stomatal opening, *Nature 414*, 656−660.
7. Huala, E., Oeller, P. W., Liscum, E., Han, I.-S., Larsen, E., and Briggs, W. R. (1997) *Arabidopsis* NPH1: a protein kinase with a putative redox-sensing domain, *Science 278*, 2120−2123.
8. Christie, J. M., Salomon, M., Nozue, K., Wada, M., and Briggs, W. R. (1999) LOV (light, oxygen, or voltage) domains of the blue-light photoreceptor phototropin (nph1): binding sites for the chromophore flavin mononucleotide, *Proc. Natl. Acad. Sci. U.S.A. 96*, 8779−8783.
9. Cheng, P., He, Q., Yang, Y., Wang, L., and Liu, Y. (2003) Functional conservation of light, oxygen, or voltage domains in light sensing, *Proc. Natl. Acad. Sci. U.S.A. 100*, 5938−5943.
10. Taylor, B. L., and Zhilin, I. B. (1999) PAS domains: internal sensors of oxygen, redox potential and light, *Microbiol. Mol. Biol. Rev. 63*, 479−506.
11. Sakai, T., Kagawa, T., Kasahara, M., Swartz, T. E., Christie, J. M., Briggs, W. R., Wada, M., and Okada, K. (2001) *Arabidopsis* nph1 and npl1: blue light receptors that mediate both phototropism and chloroplast relocation, *Proc. Natl. Acad. Sci. U.S.A. 98*, 6969−6974.
12. Mas, P., Kim, W. Y., Somers, D. E., and Kay, S. A. (2003) Targeted degradation of TOC1 by ZTL modulates circadian function in *Arabidopsis thaliana*, *Nature 426*, 567−570.
13. Jarillo, J. A., Capel, J., Tang, R. H., Yang, H. Q., Alonso, J. M., Ecker, J. R., and Cashmore, A. R. (2001) An *Arabidopsis* circadian clock component interacts with both CRY1 and phyB, *Nature 410*, 487−490.
14. Somers, D. E., Kim, W. Y., and Geng, R. (2004) The F-box protein ZEITLUPE confers dosage-dependent control on the circadian clock, photomorphogenesis, and flowering time, *Plant Cell 16*, 769−782.
15. Schultz, T. F., Kiyosue, T., Yanovsky, M., Wada, M., and Kay, S. A. (2001) A role for LKP2 in the circadian clock of *Arabidopsis*, *Plant Cell 13*, 2659−2670.
16. Fukamatsu, Y., Mitsui, S., Yasuhara, M., Tokioka, Y., Ihara, N., Fujita, S., and Kiyosue, T. (2005) Identification of LOV KELCH PROTEIN2 (LKP2)-interacting factors that can recruit LKP2 to nuclear bodies, *Plant Cell Physiol. 46*, 1340−1349.
17. Imaizumi, T., Tran, H. G., Swartz, T. E., Briggs, W. R., and Kay, S. A. (2003) FKF1 is essential for photoperiodic-specific light signalling in *Arabidopsis*, *Nature 426*, 302−306.
18. Han, L., Mason, M., Risseeuw, E. P., Crosby, W. L., and Somers, D. E. (2004) Formation of an SCF(ZTL) complex is required for proper regulation of circadian timing, *Plant J. 40*, 291−301.
19. Kuroda, H., Takahashi, N., Shimada, H., Seki, M., Shinozaki, K., and Matsui, M. (2002) Classification and expression analysis of *Arabidopsis* F-box-contaning protein genes, *Plant Cell Physiol. 43*, 1073−1085.
20. Kevei, E., Gyula, P., Hall, A., Kozma-Bognar, L., Kim, W. Y., Eriksson, M. E., Toth, R., Hanano, S., Feher, B., Southern, M. M., Bastow, R. M., Viczian, A., Hibberd, V., Davis, S. J., Somers, D. E., Nagy, F., and Millar, A. J. (2006) Forward genetic analysis of the circadian clock separates the multiple functions of ZEITLUPE, *Plant Physiol. 140*, 933−945.
21. Yanovsky, M. J., and Kay, S. A. (2002) Molecular basis of seasonal time measurement in *Arabidopsis*, *Nature 419*, 308−312.
22. Yanovsky, M. J., and Kay, S. A. (2003) Living by the calendar: how plants know when to flower, *Nat. Rev. Mol. Cell Biol. 4*, 265−275.
23. Huang, T., Bohlenius, H., Eriksson, S., Parcy, F., and Nilsson1, O. (2005) The mRNA of the *Arabidopsis* gene FT moves from leaf to shoot apex and induces flowering, *Science 309*, 1694−1696.
24. Imaizumi, T., Schultz, T. F., Harmon, F. G., Ho, L. A., and Kay, S. A. (2005) FKF1 F-box protein mediates cyclic degradation of a repressor of CONSTANS in *Arabidopsis*, *Science 309*, 293−297.
25. Johnson, E. S., Ma, P. C., Ota, I. M., and Varshavsky, A. (1995) A proteolytic pathway that recognizes ubiquitin as a degradation signal, *J. Biol. Chem. 270*, 17442−17456.
26. Ko, H. W., Jiang, J., and Edery, I. (2002) Role for Slimb in the degradation of *Drosophila* Period protein phosphorylated by Doubletime, *Nature 420*, 673−678.
27. Guo, H., and Ecker, J. R. (2003) Plant responses to ethylene gas are mediated by SCF(EBF1/EBF2)-dependent proteolysis of EIN3 transcription factor, *Cell 115*, 667−677.
28. Swartz, T. E., Corchnoy, S. B., Christie, J. M., Lewis, J. W., Szundi, I., Briggs, W. R., and Bogomolni, R. A. (2001) The photocycle of a flavin-binding domain of the blue light photoreceptor phototropin, *J. Biol. Chem. 276*, 36493−36500.
29. Corchnoy, S. B., Swartz, T. E., Lewis, J. W., Szundi, I., Briggs, W. R., and Bogomolni, R. A. (2003) Intramolecular proton transfers and structural changes during the photocycle of the LOV2 domain of phototropin 1, *J. Biol. Chem. 278*, 724−731.
30. Iwata, T., Nozaki, D., Tokutomi, S., Kagawa, T., Wada, M., and Kandori, H. (2003) Light-induced structural changes in the LOV2 domain of *Adiantum* phytochrome3 studied by low-temperature FTIR and UV−visible spectroscopy, *Biochemistry 42*, 8183−8191.
31. Nozaki, D., Iwata, T., Ishikawa, T., Todo, T., Tokutomi, S., and Kandori, H. (2004) Role of Gln1029 in the photoactivation processes of the LOV2 domain in *Adiantum* phytochrome3, *Biochemistry 43*, 8373−8379.
32. Harper, S. M., Neil, L. C., and Gardner, K. H. (2003) Structural basis of a phototropin light switch, *Science 301*, 1541−1544.
33. Eitoku, T., Nakasone, Y., Matsuoka, D., Tokutomi, S., and Terazima, M. (2005) Conformational dynamics of pPhototropin 2 LOV2 domain with the linker upon photoexcitation, *J. Am. Chem. Soc. 127*, 13238−13244.
34. Matsuoka, D., Iwata, T., Zikihara, K., Kandori, H., and Tokutomi, S. (2006) Early events in the light-signal transduction of phototropin, *Photochem. Photobiol.* (in press).
35. Kasahara, M., Swartz, T. E., Olney, M. A., Onodera, A., Mochizuki, N., Fukuzawa, H., Asamizu, E., Tabata, S., Kanegae, H., Takano, M., Christie, J. M., Nagatani, A., and Briggs, W. R. (2002) Photochemical properties of the flavin mononucleotide binding domains of the phototropins from *Arabidopsis*, rice, and *Chlamydomonas reinhardtii*, *Plant Phys. 129*, 762−773.
36. Nakasako, M., Matsuoka, D., Zikihara, K., and Tokutomi, S. (2005) Quaternary structure of LOV-domain containing polypeptides of *Arabidopsis* FKF1 protein, *FEBS Lett. 579*, 1067−1071.
37. Christie, J. M., Swartz, T. E., Bogomolni, R. A., and Briggs, W. R. (2002) Phototropin LOV domains exhibit distinct roles in regulating photoreceptor function, *Plant J. 32*, 205−219.
38. Matsuoka, D., and Tokutomi, S. (2005) Blue light-regulated molecular switch of Ser/Thr kinase in phototropin, *Proc. Natl. Acad. Sci. U.S.A. 102*, 13337−13342.
39. Yasuhara, M., Mitsui, S., Hirano, H., Takanabe, R., Tokioka, Y., Ihara, N., Komatsu, A., Seki, M., Shinozaki, K., and Kiyosue, T. (2004) Identification of ASK and clock-associated proteins as molecular partners of LKP2 (LOV kelch protein 2) in *Arabidopsis*, *J. Exp. Bot. 55*, 2015−2027.
40. Crosson, S., Rajagopal, S., and Moffat, K. (2003) The LOV domain family: photoresponsive signaling modules coupled to diverse output domains, *Biochemistry 42*, 2−10.

41. Schleicher, E., Kowalczyk, R. M., Kay, C. W. M., Hegemann, P., Bacher, A., Fischer, M., Bittl, R., Richter, G., and Weber, S. (2004) On the reaction mechanism of adduct formation in LOV domains of the plant blue-light receptor phototropin, *J. Am. Chem. Soc. 126*, 11067−11076.
42. Mincey, T., Tayrien, G., Mildvan, A. S., and Abeles, R. H. (1980) Presence of a flavin semiquinone in methanol oxidase, *Proc. Natl. Acad. Sci. U.S.A. 77*, 7099−7101.
43. Claiborne, A. (1986) Studies on the structure and mechanism of *Streptococcus faecium* L-alpha-glycerophosphate oxidase, *J. Biol. Chem. 261*, 14398−14407.
44. Ghanem, M., and Gadda, G. (2006) Effects of reversing the protein positive charge in the proximity of the flavin N(1) locus of choline oxidase, *Biochemistry 45*, 3437−3447.
45. Yagi, K., Ogura, Y., Tonomura, Y., and Nakamura, T. (1972) *Molecular Mechanisms of Enzyme Action*. p 37, University of Tokyo Press, Tokyo.
46. Yagi, K., Takai, A., and Ohishi, N. (1972) *Biochim. Biophys. Acta 289*, 37.
47. Crosson, S., and Moffat, K., (2001) Structure of a flavin-binding plant photoreceptor domain: insights into light-mediated signal transduction, *Proc. Natl. Acad. Sci. U.S.A. 98*, 2995−3000.
48. Crosson, S., and Moffat, K. (2002) Photoexcited structure of a plant photoreceptor domain reveals a light-driven molecular switch, *Plant Cell 14*, 1067−1075.
49. Fedorov, R., Schlichting, I., Hartmann, E., Domratcheva, T., Fuhrmann, M., and Hegemann, P. (2003) Crystal structures and molecular mechanism of a light-induced signaling switch: The Phot-LOV1 domain from *Chlamydomonas reinhardtii*, *Biophys. J. 84*, 2474−2482.
50. Kay, C. W., Schleicher, E., Kuppig, A., Hofner, H., Rudiger, W., Schleicher, M., Fischer, M., Bacher, A., Weber, S., and Richter, G. (2003) Blue light perception in plants. Detection and characterization of a light-induced neutral flavin radical in a C450A mutant of phototropin, *J. Biol. Chem. 278*, 10973−10982.
51. Iwata, T., Tokutomi, S., and Kandori, H. (2002) Photoreaction of the cysteine S−H group in the LOV2 domain of Adiantum phytochrome3, *J. Am. Chem. Soc. 124*, 11840−11841.
52. Salomon, M., Eisenreich, W., Dürr, H., Schleicher, E., Knieb, E., Massay, V., Rüdiger, W., Muller, F., Bacher, A., and Richter, G. (2001) An optomechanical transducer in the blue light receptor phototropin from *Avena sativa*, *Proc. Natl. Acad. Sci. U.S.A. 98*, 12357−12361.
53. Iwata, T., Nozaki, D., Tokutomi, S., and Kandori, H. (2005) Comparative investigation of the LOV1 and LOV2 domains in *Adiantum* phytochrome3, *Biochemistry 44*, 7427−7434.
54. Nozaki, D., Iwata, T., Tokutomi, S., and Kandori, H. (2005) Unique temperature dependence in the adduct formation between FMN and cysteine S−H group in the LOV2 domain of *Adiantum* phytochrome3, *Chem. Phys. Lett. 410*, 59−63.
55. Sato, Y., Iwata, T., Tokutomi, S., and Kandori, H. (2005) Reactive cysteine is protonated in the triplet excited state of the LOV2 domain in adiantum phytochrome3, *J. Am. Chem. Soc. 127*, 1088−1089.

BI0607857

4406–4415 *Nucleic Acids Research, 2006, Vol. 34, No. 16* *Published online 26 August 2006*
doi:10.1093/nar/gkl572

Chemical synthesis of oligodeoxyribonucleotides containing the Dewar valence isomer of the (6–4) photoproduct and their use in (6–4) photolyase studies

Junpei Yamamoto[1], Kenichi Hitomi[1,2], Takeshi Todo[3] and Shigenori Iwai[1,*]

[1]Division of Chemistry, Graduate School of Engineering Science, Osaka University, 1-3 Machikaneyama, Toyonaka, Osaka 560-8531, Japan, [2]Department of Molecular Biology and the Skaggs Institute for Chemical Biology, The Scripps Research Institute, 10550 North Torrey Pines Road, La Jolla, CA 92037, USA and [3]Radiation Biology Center, Kyoto University, Yoshidakonoe-cho, Sakyo-ku, Kyoto 606-8501, Japan

Received April 8, 2006; Revised July 14, 2006; Accepted July 20, 2006

ABSTRACT

The pyrimidine(6–4)pyrimidone photoproduct, a major UV lesion formed between adjacent pyrimidine bases, is transformed to its Dewar valence isomer upon exposure to UVA/UVB light. We have synthesized a phosphoramidite building block of the Dewar photoproduct formed at the thymidylyl (3′–5′)thymidine site and incorporated it into oligodeoxyribonucleotides. The diastereoisomers of the partially protected dinucleoside monophosphate bearing the (6–4) photoproduct, which were caused by the chirality of the phosphorus atom, were separated by reversed-phase chromatography, and the (6–4) photoproduct was converted to the Dewar photoproduct by irradiation of each isomer with Pyrex-filtered light from a high-pressure mercury lamp. The Dewar photoproduct was stable under both acidic and alkaline conditions at room temperature. After characterization of the isomerized base moiety by NMR spectroscopy, a phosphoramidite building block was synthesized in three steps. Although the ordinary method could be used for the oligonucleotide synthesis, benzimidazolium triflate as an alternative activator yielded better results. The oligonucleotides were used for the analysis of the reaction and the binding of *Xenopus* (6–4) photolyase. Although the affinity of this enzyme for the Dewar photoproduct-containing duplex was reportedly similar to that for the (6–4) photoproduct-containing substrate, the results suggested a difference in the binding mode.

INTRODUCTION

Ultraviolet (UV) light causes two major types of photolesions, namely *cis–syn* cyclobutane pyrimidine dimers (CPDs) and pyrimidine(6–4)pyrimidone photoproducts [(6–4) photoproducts, 2], at dipyrimidine sites (1) in DNA. The (6–4) photoproduct is converted to another product, originally designated as TpT3, by irradiation at 313 nm (1). A structural analysis of TpT3 revealed that the 2-pyrimidone ring of the (6–4) photoproduct was photoisomerized to a Dewar-type structure (3) (2), as shown in Scheme 1, and since then, the isomerized product has been called the Dewar valence isomer or the Dewar photoproduct. In addition to the isomerization of the isolated (6–4) photoproduct (3,4), the Dewar photoproducts are formed by the UVB irradiation of the original pyrimidine dinucleoside monophosphates (5,6) or DNA (7). They are reportedly detected in the DNA of mammalian cells exposed to simulated or natural sunlight (8–10). Reversion of the Dewar valence isomer to the (6–4) photoproduct by far-UV irradiation was also described previously (1,11).

The conformation of the Dewar photoproduct of thymidylyl(3′–5′)thymidine was determined by NMR spectroscopy and molecular modeling, and was found to be similar to that of the (6–4) photoproduct. However, the 3′ component of the Dewar photoproduct, i.e. 5-methyl-2-oxo-1,3-diazabicyclo[2.2.0]hex-5-ene, is not planar, unlike the 3′ base of the (6–4) photoproduct (3). This difference affects the thermodynamic properties of the base pair formation and the mutation spectra. While duplexes with guanine opposite the 3′ component of the (6–4) photoproduct are thermodynamically more stable than those with adenine, this stabilization is reduced by the isomerization to the Dewar photoproduct, although the functional groups are the same in these two photoproducts (12,13). The (6–4) photoproduct formed at the TT sequence causes a T→C transition mutation at the 3′ pyrimidone with an extremely high frequency in SOS-induced *Escherichia coli* cells, but its Dewar valence isomer shows lower mutation frequency and specificity (14,15). The human damaged DNA-binding protein, which recognizes DNA containing the (6–4) photoproduct (16) and initiates global genome nucleotide excision repair (17), binds DNA containing the Dewar valence isomer with high affinity (18), and it was demonstrated that the Dewar photoproduct

*To whom correspondence should be addressed. Tel: +81 6 6850 6250; Fax: +81 6 6850 6240; Email: iwai@chem.es.osaka-u.ac.jp

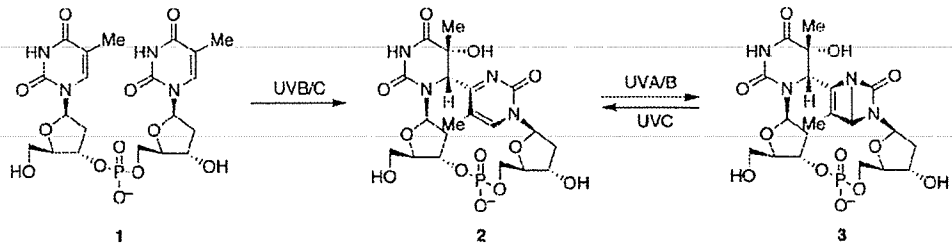

Scheme 1. The (6–4) photoproduct (**2**) and its Dewar valence isomer (**3**) formed at the TT site (**1**).

was repaired as efficiently as the (6–4) photoproduct in human cells, probably via the nucleotide excision repair pathway (19). Another repair enzyme, the (6–4) photolyase (20), also binds DNA containing the Dewar photoproduct, although its affinity for this damaged DNA is slightly lower than that for the (6–4) photoproduct-containing DNA. The dissociation constants reported for the (6–4) and Dewar photoproducts are 5.0×10^{-10} and 1.4×10^{-9} M, respectively (21). However, the repair of the Dewar isomer to the original pyrimidines by the (6–4) photolyase is extremely slow, and the reported quantum yield is 0.5% of that obtained for the repair of the (6–4) photoproduct (21).

For biochemical studies, oligonucleotides containing the Dewar photoproduct have been prepared by two steps. Short oligonucleotides containing a single TT sequence were first irradiated at 254 nm, and the resultant products containing the (6–4) photoproduct were purified by high-performance liquid chromatography (HPLC). Subsequently, the (6–4) photoproduct in these oligonucleotides was converted to its Dewar valence isomer by a second irradiation step at longer wavelengths (12,14,22). A problem in this method, however, is that the HPLC separation of the oligonucleotide containing the Dewar photoproduct from the starting material containing the (6–4) photoproduct is very difficult, even though the oligonucleotide is short (12,22). Although the Dewar photoproduct is photoequilibrated with the (6–4) photoproduct in irradiated cells, oligonucleotides free from contamination with the isomerized form are required for *in vitro* studies, and the 100% purity is not guaranteed for the samples prepared by the post-synthetic irradiation method. For the CPD and the (6–4) photoproduct, methods for the chemical synthesis of oligonucleotides using the dinucleotide-type phosphoramidite building blocks have been developed previously (23–26), and the photolesion-containing oligonucleotides synthesized by this method have been used for various biochemical studies including translesion replication (27–30), which requires extremely pure template oligonucleotides. Here we describe the extension of this synthetic method to the Dewar photoproduct, which enables us to obtain the Dewar photoproduct-containing oligonucleotides without any contamination with the (6–4) photoproduct, and its application to the analysis of a repair enzyme, (6–4) photolyase.

MATERIALS AND METHODS

General methods

All solvents and reagents were obtained from Wako Pure Chemical Industries, Ltd. (Osaka, Japan). Reagents for the DNA synthesizer were purchased from Applied Biosystems Japan (Tokyo, Japan) and Glen Research (Sterling, VA). TLC analyses were carried out on Merck Silica gel 60 F_{254} plates, which were visualized by UV illumination at 254 nm. For column chromatography, Wakogel C-200 (Wako Pure Chemical Industries) was used. For reversed-phase chromatography, Prep C18 55–105 μm 125 Å resin (Waters Corporation, Milford, MA) was used on a Bio-Rad Econo System. UV and fluorescence spectra were recorded on a Shimadzu BioSpec-mini spectrophotometer and a Shimadzu RF-5300PC spectrofluorophotometer, respectively. ^{1}H and ^{31}P NMR spectra were measured on Varian INOVA 600 and JEOL GSX270 spectrometers, respectively. Tetramethylsilane and trimethyl phosphate were used as internal standards. Proton signals were assigned by using homonuclear 2D NMR techniques, correlation spectroscopy (COSY) and rotating frame Overhauser effect spectroscopy (ROESY). The ROESY spectra were measured with a mixing time of 800 ms. Mass spectra were obtained on a Hitachi M-4000H spectrometer. HPLC analyses were carried out on a Gilson gradient-type analytical system equipped with a Waters 2996 photodiode array detector, and a Waters μBondasphere C18 5μm 300 Å column (3.9 mm × 150 mm) was used at a flow rate of 1.0 ml/min with a linear gradient of acetonitrile in 0.1 M triethylammonium acetate (pH 7.0). Matrix-assisted laser desorption/ionization time-of-flight (MALDI-TOF) mass spectra of oligonucleotides were measured in the negative ion mode on an Applied Biosystems Voyager DE PRO spectrometer, using 3-hydroxypicolinic acid as a matrix.

Conversion of the (6–4) photoproduct (4a, 4b) to its Dewar valence isomer (5a, 5b)

The dinucleoside monophosphate of the (6–4) photoproduct (**4a**, **4b**) was purified on a column of alkylated silica gel (1.5 cm × 48 cm) with a linear gradient of 10–25% aqueous acetonitrile for 400 min, after the UV irradiation described previously (25). The separated compounds (**4a**, 191 mg, 273 μmol; **4b**, 371 mg, 532 μmol) were dissolved in 20% aqueous acetonitrile (1.2 l), and after nitrogen bubbling for 10 min, each solution was irradiated in a Pyrex immersion well apparatus fitted with a 450 W high-pressure mercury lamp (UM-452; Ushio, Tokyo, Japan) in a 5°C water bath (NCB-2200; EYELA, Tokyo, Japan) for 1 h. The products (**5a** and **5b**) were purified separately on the same column with an acetonitrile gradient of 10–17.5% (**5a**) or 10–25% (**5b**) for 400 min, and the fractions were analyzed by reversed-phase HPLC with an acetonitrile gradient from

11 to 17% for 15 min. The fractions containing the product without UV absorption in the long wavelength region were collected, and a glassy solid was obtained after evaporation. **5a**: Yield 94 mg (134 μmol, 49%). ^{1}H-NMR (pyridine-d_5) δ (p.p.m.) 12.64 (s, 1H, –NH–), 7.02 (dd, J = 1.9, 9.5 Hz, 1H, Tp H1′), 5.62 (m, 2H, pT H1′, Tp H6), 5.50 (m, 1H, Tp H3′), 5.32 (m, 1H, pT H3′), 4.94 (s, 1H, pT H6), 4.60 (m, 3H, pT H5′, –OCH_2CH$_2$CN), 4.44 (m, 1H, pT H5″), 4.33 (dd, J = 2.0, 12.2 Hz, 1H, Tp H5′), 4.12 (m, 2H, pT H4′, Tp H5″), 4.01 (m, 1H, Tp H4′), 3.28 (m, 1H, Tp H2′), 3.12 (m, 2H, –OCH$_2$CH_2CN), 2.84–2.56 (m, 5H, –OCOCH_2CH_2CO–, Tp H2″), 2.38 (s, 3H, pT, –CH$_3$), 2.19 (m, 2H, pT H2′, pT H2″), 2.07 (s, 3H, –COCH$_3$), 1.84 (s, 3H, Tp, –CH$_3$). ^{31}P-NMR (pyridine-d_5) δ –6.39 p.p.m. HRMS (SI) m/z 720.1889 ([M+Na]$^+$; calcd for $C_{28}H_{36}N_5O_{14}$PNa, 720.1891). **5b**: Yield 247 mg (339 μmol, 67%). ^{1}H-NMR (pyridine-d_5) δ (p.p.m.) 12.61 (s, 1H, –NH–), 7.06 (d, J = 9.1 Hz, 1H, Tp H1′), 5.72 (s, 1H, Tp H6), 5.70 (t, J = 8.6 Hz, 1H, Tp H3′), 5.65 (dd, J = 5.6, 9.5 Hz, 1H, pT H1′), 5.17 (m, 1H, pT H3′), 4.96 (s, 1H, pT H6), 4.60 (m, 1H, pT H5′), 4.54 (m, 1H, pT H5″), 4.44 (m, 2H, –OCH_2CH$_2$CN), 4.32 (d, J = 10.7 Hz, 1H, Tp H5′), 4.22 (d, J = 10.9 Hz, 1H, Tp H5″), 4.12 (m, 1H, pT H4′), 4.03 (d, J = 7.9 Hz, 1H, Tp H4′), 3.26 (dd, J = 8.6, 14.2 Hz, 1H, Tp H2′), 3.02 (t, J = 6.1 Hz, 2H, –OCH$_2$CH_2CN), 2.77 (m, 2H, –OCOCH$_2$CH_2CO–), 2.68–2.58 (m, 3H, –OCOCH_2CH$_2$CO–, Tp H2″), 2.36 (s, 3H, pT, –CH$_3$), 2.13 (m, 2H, pT H2′, pT H2″), 2.07 (s, 3H, –COCH$_3$), 1.91 (s, 3H, Tp, –CH$_3$). ^{31}P-NMR (pyridine-d_5) δ –3.27 p.p.m. HRMS (SI) m/z 720.1896 ([M+Na]$^+$; calcd for $C_{28}H_{36}N_5O_{14}$PNa, 720.1891).

Protection of the 5′-OH function (6a and 6b)

The partially protected dinucleoside monophosphate of the Dewar photoproduct (**5a**, 171 mg, 245 μmol) was dissolved in pyridine (3 ml) and was mixed with 4,4′-dimethoxytrityl (DMT) chloride (211 mg, 623 μmol). After stirring at room temperature for 3 h, methanol (1.0 ml) was added and the mixture was concentrated. The residue was dissolved in chloroform (30 ml), washed with water and was chromatographed, after concentration and coevaporation with toluene, on silica gel with a step gradient of 0–4% methanol in chloroform. The fractions containing the tritylated product were collected, and **6a** was obtained as a foam after evaporation. The other isomer (**5b**, 218 mg, 313 μmol) was treated in the same way. **6a**: Yield 204 mg (204 μmol, 83%). ^{1}H-NMR (CDCl$_3$) δ (p.p.m.) 7.67 (br, 1H, –NH–), 7.43 (d, J = 4.1 Hz, 2H, aromatic), 7.30 (m, 6H, aromatic), 7.24 (t, J = 7.3 Hz, 1H, aromatic), 6.84 (d, J = 4.4 Hz, 4H, aromatic), 6.45 (dd, J = 2.8, 9.7 Hz, 1H, Tp H1′), 5.56 (dd, J = 6.1, 8.5 Hz, 1H, pT H1′), 5.08 (m, 1H, pT H3′), 5.00 (s, 1H, pT H6), 4.73 (m, 1H, Tp H3′), 4.65 (s, 1H, Tp H6), 4.37 (d, J =11.0 Hz, 1H, pT H5′), 4.09 (m, 2H, pT H5″, –OCH_2CH$_2$CN), 3.95 (m, 1H, pT H4′), 3.82 (m, 2H, Tp H4′, –OCH_2CH$_2$CN), 3.79 (s, 6H, –OCH$_3$), 3.72 (dd, J = 2.6, 11.0 Hz, 1H, Tp H5′), 3.48 (br, 1H, –OH), 3.24 (dd, J = 2.9, 11.0 Hz, 1H, Tp H5″), 2.86 (m, 1H, Tp H2′), 2.81–2.71 (m, 2H, –OCOCH$_2$CH_2CO–), 2.65–2.49 (m, 3H, –OCH$_2$CH_2CN, –OCOCH_2CH$_2$CO–), 2.40–2.28 (m, 3H, Tp H2″, pT H2′, –OCH$_2$CH_2CN), 2.19 (s, 3H, –COCH$_3$), 2.09 (m, 1H, pT H2″), 2.01 (s, 3H, pT –CH$_3$), 1.51 (s, 3H, Tp –CH$_3$). ^{31}P-NMR (CDCl$_3$) δ –6.85 p.p.m. HRMS (SI) m/z 1022.3202 ([M+Na]$^+$; calcd for $C_{49}H_{54}N_5O_{16}$PNa, 1022.3197). **6b**: Yield 297 mg (297 μmol, 95%). ^{1}H-NMR (CDCl$_3$) δ (p.p.m.) 7.79 (br, 1H, –NH–), 7.47 (d, J = 8.1 Hz, 2H, aromatic), 7.38 (dd, J = 2.0, 8.9 Hz, 4H, aromatic), 7.30 (t, J = 7.8 Hz, 2H, aromatic), 7.20 (t, J = 7.4 Hz, 1H, aromatic), 6.84 (d, J = 8.8 Hz, 4H, aromatic), 6.43 (dd, J = 2.6, 9.7 Hz, 1H, Tp H1′), 5.53 (dd, J = 4.7, 10.3 Hz, 1H, pT H1′), 5.01 (m, 1H, Tp H3′), 4.96 (s, 1H, pT H6), 4.83 (m, 2H, Tp H6, pT H3′), 4.31 (m, 1H, pT H5′), 4.21 (m, 1H, pT H5″), 4.04–3.89 (m, 3H, pT H4′, –OCH_2CH$_2$CN), 3.78 (s, 6H, –OCH$_3$), 3.72 (d, J = 8.3 Hz, 1H, Tp H4′), 3.69 (dd, J = 2.4, 11.1 Hz, 1H, Tp H5′), 3.64 (br, 1H, –OH), 3.11 (dd, J = 2.6, 11.2 Hz, 1H, Tp H5″), 2.75 (m, 3H, Tp H2′, –OCOCH$_2$CH_2CO–), 2.64–2.49 (m, 4H, –OCH$_2$CH_2CN, –OCOCH_2CH$_2$CO–), 2.30–2.20 (m, 2H, Tp H2″, pT H2′), 2.18 (s, 3H, –COCH$_3$), 1.94 (m, 1H, pT H2″), 1.90 (s, 3H, pT –CH$_3$), 1.62 (s, 3H, Tp –CH$_3$). ^{31}P-NMR (CDCl$_3$) δ –3.44 p.p.m. HRMS (SI) m/z 1022.3190 ([M+Na]$^+$; calcd for $C_{49}H_{54}N_5O_{16}$PNa, 1022.3197).

Removal of the levulinyl group (7a and 7b)

The protected dinucleoside monophosphate of the Dewar photoproduct (**6a**, 181 mg, 181 μmol) was dissolved in pyridine (2.3 ml), and a solution (2.3 ml) of hydrazine monohydrate (88 μl, 1.8 mmol) in pyridine-acetic acid (3:2, v/v) was added. After stirring at room temperature for 5 min, the mixture was cooled in an ice bath, and acetone (2.0 ml) was added. The mixture was diluted with chloroform (30 ml), washed with 2% aqueous NaHCO$_3$ and with water, dried with Na$_2$SO$_4$ and concentrated. After coevaporation with toluene, the residue was chromatographed on silica gel (4.8 g) with a step gradient of 0–5% methanol in chloroform and a product (**7a**) was obtained as a glassy solid after evaporation. The other isomer (**6b**, 454 mg, 454 μmol) was treated in the same way. **7a**: Yield 151 mg (167 μmol, 92%). ^{1}H-NMR (DMSO-d_6) δ (p.p.m.) 10.46 (s, 1H, –NH–), 7.40 (d, J = 7.7 Hz, 2H, aromatic), 7.26 (m, 7H, aromatic), 6.88 (dd, J = 2.6, 9.2 Hz, 4H, aromatic), 6.29 (dd, J = 2.8, 9.8 Hz, 1H, Tp H1′), 5.92 (br, 1H, Tp –OH), 5.41 (m, 2H, pT H1′, 3′-OH), 5.21 (s, 1H, pT H6), 4.46 (m, 1H, Tp H3′), 4.25 (s, 1H, Tp H6), 4.18 (m, 1H, pT H5′), 4.10 (m, 1H, pT H3′), 3.94 (m, 2H, pT H5″, –OCH_2CH$_2$CN), 3.81 (m, 1H, Tp H4′), 3.74 (m, 7H, –OCH_2CH$_2$CN, –OCH$_3$), 3.65 (m, 1H, pT H4′), 2.77 (m, 1H, Tp H2′), 2.69 (m, 2H, –OCH$_2$CH_2CN), 2.11 (m, 2H, Tp H2″, pT H2′), 2.00 (m, 1H, pT H2″), 1.88 (s, 3H, pT –CH$_3$), 1.39 (s, 3H, Tp –CH$_3$). ^{31}P-NMR (DMSO-d_6) δ –6.75 p.p.m. HRMS (SI) m/z 924.2824 ([M+Na]$^+$; calcd for $C_{44}H_{48}N_5O_{14}$PNa, 924.2829). **7b**: Yield 392 mg (435 μmol, 96%). ^{1}H-NMR (DMSO-d_6) δ (p.p.m.) 10.46 (s, 1H, –NH–), 7.42 (d, J = 8.3 Hz, 2H, aromatic), 7.30 (m, 6H, aromatic), 7.22 (t, J = 7.3 Hz, 1H, aromatic), 6.87 (dd, J = 2.8, 9.2 Hz, 4H, aromatic), 6.25 (dd, J = 2.8, 9.7 Hz, 1H, Tp H1′), 6.00 (br, 1H, Tp –OH), 5.40 (m, 2H, pT H1′, 3′-OH), 5.21 (s, 1H, pT H6), 4.93 (m, 1H, Tp H3′), 4.42 (s, 1H, Tp H6), 4.19 (d, J = 10.8 Hz, 1H, pT H5′), 4.00 (m, 4H, pT H3′, pT H5″, –OCH_2CH$_2$CN), 3.74 (m, 8H, Tp H4′, pT H4′, –OCH$_3$), 3.40 (d, J = 10.7 Hz, 1H, Tp H5′), 3.06 (dd, J = 2.9, 11.3 Hz, 1H, Tp H5″), 2.83 (m, 2H, –OCH$_2$CH_2CN),

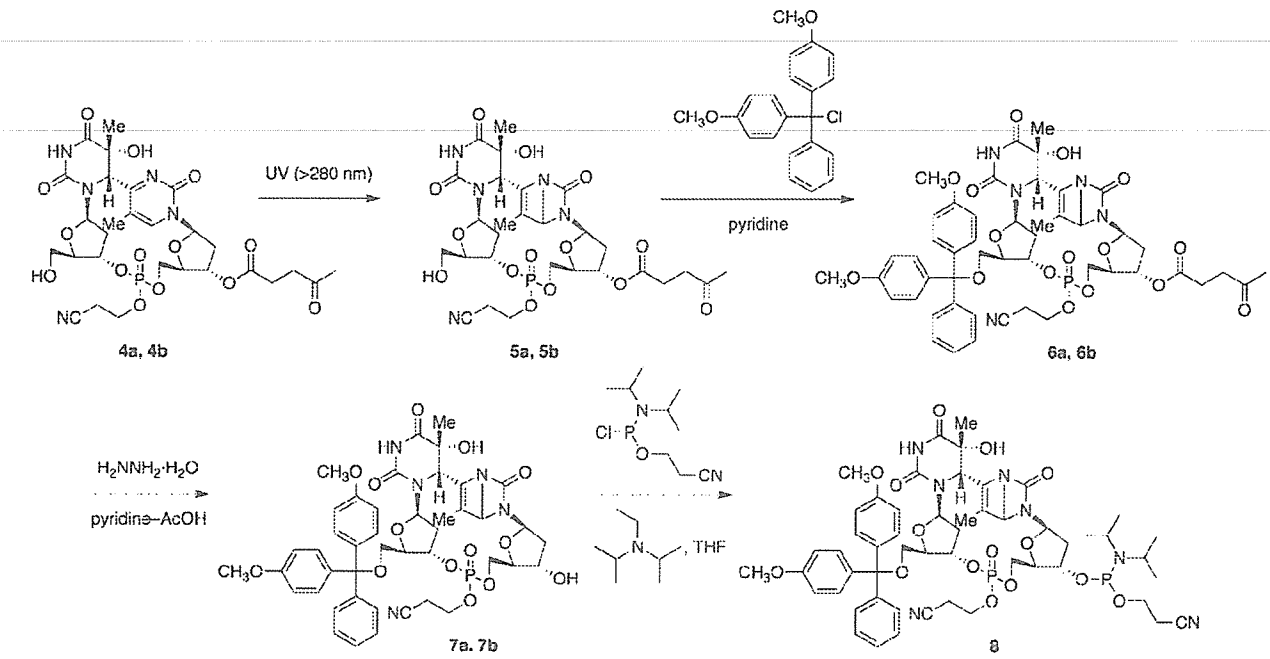

Scheme 2. Synthesis of the building block of the Dewar photoproduct.

2.64 (m, 1H, Tp H2′), 2.15 (m, 1H, Tp H2″), 1.97 (m, 2H, pT H2′, pT H2″), 1.84 (s, 3H, pT $-CH_3$), 1.38 (s, 3H, Tp $-CH_3$). ^{31}P-NMR (DMSO-d_6) δ −3.29 p.p.m. HRMS (SI) *m/z* 924.2831 ($[M+Na]^+$; calcd for $C_{44}H_{48}N_5O_{14}PNa$, 924.2829).

Phosphoramidite building block of the Dewar photoproduct (8)

An aliquot of **7b** (165 mg, 183 μmol) was mixed with tetrahydrofuran (1.6 ml) and *N*, *N*-diisopropylethylamine (127 μl, 732 μmol) and 2-cyanoethyl *N*,*N*-diisopropylchlorophosphoramidite (82 μl, 336 μmol) was added. This mixture was stirred at room temperature for 30 min and diluted with ethyl acetate (40 ml). The resulting solution was washed with 2% aqueous $NaHCO_3$ and with water, dried with Na_2SO_4, concentrated to a gum and coevaporated with toluene. The residue was chromatographed on silica gel (5 g) with a step gradient of 0–2% methanol in ice-cooled chloroform containing 0.5% pyridine. The appropriate fractions were collected and concentrated. The residue was dissolved in chloroform (1 ml) and was precipitated in pentane (20 ml), and the precipitate was washed with pentane. Yield 166 mg (151 μmol, 83%). ^{31}P-NMR ($CDCl_3$) δ (p.p.m.) 147.04, 146.69, −3.29, −3.53. HRMS (SI) *m/z* 1124.3919 ($[M+Na]^+$; calcd for $C_{53}H_{65}N_7O_{15}P_2Na$, 1124.3908).

Oligonucleotide synthesis

The phosphoramidite building block of the Dewar photoproduct (8) was dissolved in anhydrous acetonitrile at a concentration of 0.13 M and was installed on an Applied Biosystems 3400 DNA synthesizer. Nucleoside phosphoramidites for ultramild DNA synthesis (Glen Research), as well as the base-unprotected thymidine phosphoramidite, were also dissolved in acetonitrile to make 0.1 M solutions and were installed on the synthesizer. Oligonucleotides were synthesized on a 0.2 μmol scale, and the reaction time for the coupling of the Dewar photoproduct building block was prolonged to 20 min. For the synthesis using benzimidazolium triflate (BIT) as an activator, a 0.2 M solution was prepared to replace the tetrazole solution, and a polystyrene support (Universal Support II PS, Glen Research) was used without changing the synthesis procedure. After chain assembly and removal of the 5′-terminal DMT group on the synthesizer, the solid supports containing the oligonucleotides were treated with 28% aqueous ammonia (2 ml) at room temperature for 2 h. The resulting ammoniac solutions were concentrated to dryness on a rotary evaporator equipped with a vacuum pump. The residues were dissolved in water (1 ml) and the oligonucleotides were analyzed and purified by HPLC. The column was heated to 50°C and the acetonitrile gradients were 5–11, 6–12 and 8–13% for 20 min in the cases of the 12mer, 20mer and 30mer, respectively. After purification, the HPLC analysis of the 12mer was performed at room temperature using an acetonitrile gradient from 7 to 13% for 20 min.

Analysis of the (6–4) photolyase reaction

Solutions (180 μl) of *Xenopus laevis* (6–4) photolyase (31) (2 nmol), in a buffer containing 10 mM Tris–HCl (pH 8.0) and 2 mM 2-mercaptoethanol, were covered with a Pyrex lid and were irradiated on ice with an 18 W fluorescent lamp at a distance of 15 cm for 30 min. A solution (20 μl) of the 12mer containing the (6–4) or Dewar photoproduct (0.2 nmol) was added, and the mixtures were irradiated again for 3 or 24 h. After heating to 80°C for 30 min, the mixtures were passed through a NAP-5 column (Amersham Biosciences AB, Uppsala, Sweden), and the eluates were

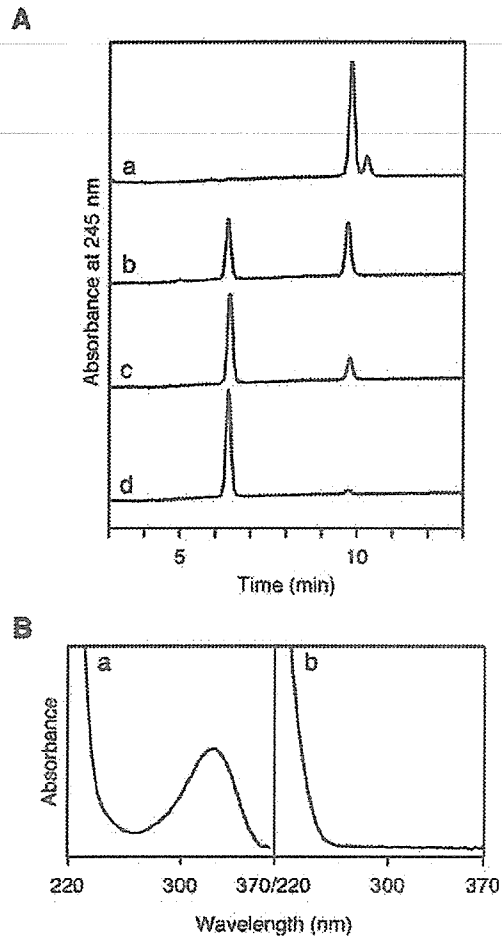

Figure 1. (A) Formation of the Dewar photoproduct. The dinucleoside monophosphate of the (6–4) photoproduct (2) was irradiated with Pyrex-filtered light from a 100 W high-pressure mercury lamp for 0 h (a), 1 h (b), 2 h (c) and 4 h (d), and the samples were analyzed by HPLC, using an acetonitrile gradient from 0 to 5% for 16 min. (B) Absorption spectra of 2 (a) and the irradiation product (b). The absorption spectra of the two peaks of trace b in (A) were extracted with the data processing software for the photodiode array detector.

analyzed by HPLC under the same conditions as those used for the analysis of the purified 12mer.

Analysis of the binding of (6–4) photolyase

The 20mer containing the Dewar photoproduct (Dw), d(CCTACGCAAAT-Dw-GGCATCC), was hybridized to a complementary strand containing 2-aminopurine (Ap), d(GGATGCC-Ap-AATTTGCGTAGG), by heating a mixture (40 µl) of the two oligonucleotides (1.2 nmol each) to 80°C for 3 min and cooling it to room temperature. A duplex without the photoproduct was prepared in the same way. These duplexes were dissolved at 0.3 µM in a buffer containing 50 mM Tris–HCl (pH 8.0), 50 mM NaCl, 1 mM 2-mercaptoethanol and 10% glycerol, and fluorescence spectra were measured at 5°C, in the absence or presence of 350 nM *X.laevis* (6–4) photolyase. The excitation wavelength was 313 nm. Experiments using the undamaged and (6–4) photoproduct-containing duplexes were performed in the same way.

RESULTS AND DISCUSSION

Formation and stability of the Dewar photoproduct

We intended to synthesize oligonucleotides containing the Dewar photoproduct formed at the TT sequence (3) using a dinucleotide building block, to extend our previous studies on the (6–4) photoproduct (25,26). Before the preparation of the building block, we analyzed the formation and the stability of the Dewar photoproduct. A solution of the dinucleoside monophosphate of the (6–4) photoproduct (2), which was obtained by deprotection of the intermediate in the preparation of the (6–4) photoproduct building block (a mixture of compounds **4a** and **4b** in Scheme 2), was irradiated on ice in a petri dish with a Pyrex lid using a 100 W high-pressure mercury lamp covered with a Pyrex water jacket. HPLC analysis of the irradiated solution on a reversed-phase column is shown in Figure 1A. A new peak emerged, and the (6–4) photoproduct was converted to this product almost completely in 4 h. We assigned this product as the Dewar valence isomer (3) because the absorption at wavelengths longer than 260 nm was lost (Figure 1B), as reported for the Dewar photoproduct (1,32).

The dinucleoside monophosphate of the Dewar photoproduct formed in the above experiment was used to analyze its stability. Compound 3 was treated with acetic acid at room temperature for 1 h to confirm that the damaged base would not be degraded during the DMT removal step in every cycle of oligonucleotide synthesis. Another experiment was its treatment with aqueous ammonia at room temperature for 2 h, which is used for the deprotection of oligonucleotides synthesized by the 'ultramild' method. The latter analysis is very important, because the Dewar isomer is reportedly more labile than the (6–4) photoproduct under alkaline conditions (11,22). HPLC analysis of the reaction mixtures revealed that the Dewar photoproduct was stable under both of these conditions, although a very small peak was detected at a short retention time after the ammonia treatment (Supplementary Figure 1).

The phosphoramidite building block of the Dewar photoproduct

Although the Dewar photoproduct can be obtained directly by irradiation of thymidylyl(3′–5′)thymidine at wavelengths longer than 280 nm, its yield by this method is very low (2). Therefore, the (6–4) photoproduct prepared by our previous method (25) was isomerized in this study. After the formation of the (6–4) photoproduct by irradiation of the protected thymidylyl(3′–5′)thymidine with germicidal lamps, the diastereomers caused by the chirality of the phosphorus atom were separated by reversed-phase chromatography on alkylated silica gel, as described previously (25). The isomers with shorter and longer retention times in reversed-phase HPLC analysis were designated as **4a** and **4b**, respectively. Each diastereomer of the dinucleoside monophosphate was dissolved in 20% aqueous acetonitrile and was irradiated at 5°C in a Pyrex immersion well apparatus fitted with a

450 W high-pressure mercury lamp. At intervals of 10 min, aliquots of the solution were analyzed by reversed-phase HPLC, and the decrease of the starting material, as determined from the peak areas of the chromatograms at 325 nm, was monitored (Supplementary Figure 2). After 70 min, the (6–4) photoproduct was consumed almost completely and was converted to a single product, which did not absorb UV light with wavelengths longer than 280 nm (Figure 2A). The same results were obtained regardless of the stereochemistry of the phosphotriester linkage. Aliquots of the products were treated with aqueous ammonia at room temperature for 2 h for deprotection and were subjected to HPLC analysis. As shown in Figure 2B, the deprotected products were identical to the authentic sample of the Dewar photoproduct obtained by irradiation of the deprotected (6–4) photoproduct (trace d in Figure 1A).

The putative Dewar-containing dinucleoside monophosphates (**5a** and **5b**) were purified separately by reversed-phase chromatography and were analyzed by ^{1}H-NMR spectroscopy. The proton signals were assigned using COSY and ROESY spectra, and as reported for the Dewar photoproduct without the protecting groups (3), ROESY crosspeaks were observed between pT CH_3 and Tp H3′ and between pT CH_3 and pT H3′ for both **5a** and **5b**. It was also reported that the conversion of the (6–4) photoproduct to its Dewar valence isomer resulted in an up-field shift of the H6 signal of the 3′ base moiety (3). In the present study, the chemical shifts of H6 were 7.84, 8.01, 4.94 and 4.96 for **4a**, **4b**, **5a** and **5b**, respectively. This observation, together with the HPLC analysis shown in Figure 2B, the UV absorption spectra and the molecular weight determined by high-resolution mass spectrometry, demonstrated that the obtained products were the dinucleoside monophosphates of the Dewar photoproduct.

The dinucleoside monophosphates bearing the Dewar photoproduct (**5a** and **5b**) were converted to the 5′-DMT derivatives (**6a** and **6b**) before the removal of the 3′-protecting group to yield **7a** and **7b**, in the same way as described for

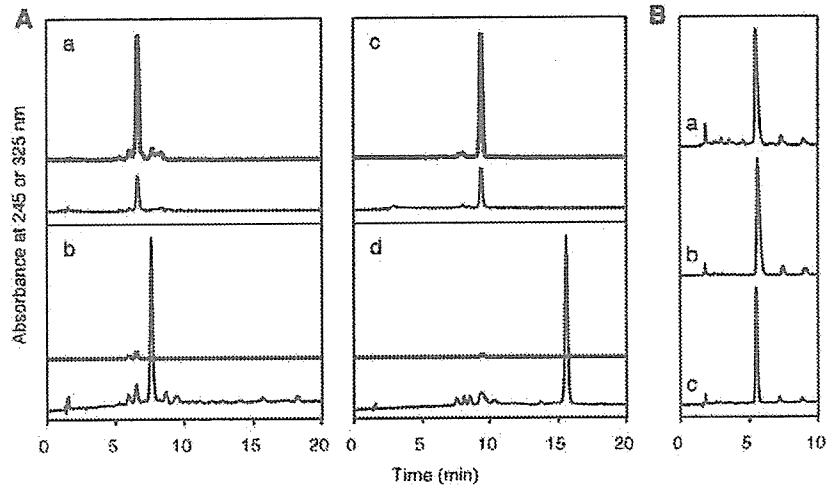

Figure 2. (A) Conversion of **4a** and **4b** to **5a** and **5b**. Compounds **4a** (a) and **4b** (c) were irradiated with a 450 W high-pressure mercury lamp for 1 h, and the starting materials (a and c) and the reaction mixtures (b and d) were analyzed by HPLC, using an acetonitrile gradient from 11 to 17% for 20 min. The thick and thin lines show the chromatograms monitored at 325 and 245 nm, respectively. (B) Deprotection of **5a** and **5b**. Aliquots of **5a** and **5b** were treated with aqueous ammonia at room temperature for 2 h, and were analyzed by HPLC after evaporation (a and b, respectively). (c) A mixture of the deprotected compounds was co-injected with the authentic Dewar photoproduct (trace d in Figure 1A). The acetonitrile gradient was the same as that described in the legend to Figure 1A.

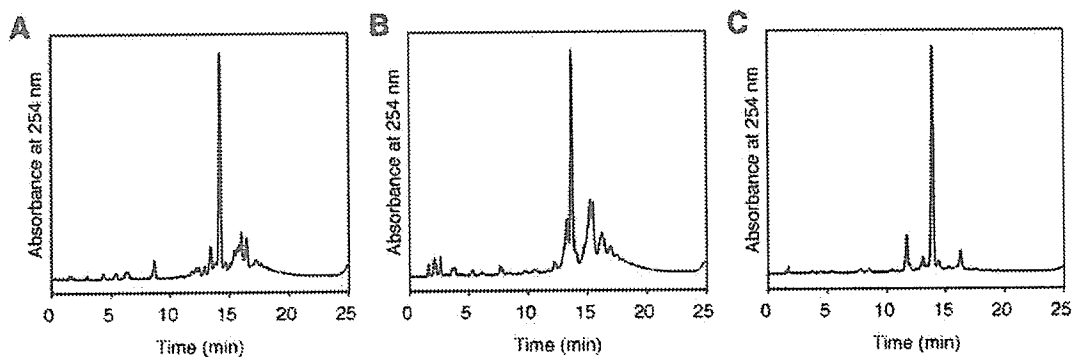

Figure 3. Reversed-phase HPLC analysis of crude oligonucleotides after deprotection. (A and B) The 20mer (A) and the 30mer (B) synthesized by the ordinary method using tetrazole. (C) The 20mer synthesized by the BIT-activation method. The HPLC conditions are described in Materials and Methods.

the (6–4) photoproduct (25). Since the obtained amount of **7b** was 2.6-fold larger than that of **7a**, **7b** was used for the preparation of the phosphoramidite building block. After the phosphitylation of **7b**, we tried to purify the phosphoramidite building block of the Dewar photoproduct (**8**) by chromatography on silica gel using a solvent system of chloroform–methanol containing 0.1% pyridine, as developed for the (6–4) photoproduct. However, a ^{31}P-NMR measurement revealed that the phosphoramidite was degraded during this chromatographic purification. Both of the phosphoramidite signals were diminished, and a new signal emerged at 11.66 p.p.m. The degradation was reproducible and also occurred when **7a** was used. This result suggested that the phosphoramidite moiety attached to the dinucleoside monophosphate of the Dewar photoproduct is more labile than those in other building blocks. After testing several solvent systems, we found that the phosphoramidite could be obtained in an intact form by flash chromatography using chloroform containing 0.5% pyridine.

In this study, the two phosphorus diastereomers were separated at the initial stage, in order to characterize the intermediates by NMR spectroscopy, but it is possible to use a mixture of the diastereomers as we are practicing in the case of the (6–4) photoproduct.

Synthesis of oligonucleotides containing the Dewar photoproduct

Using the phosphoramidite building block of the Dewar photoproduct (**8**) prepared as above, a 12mer, d(CA-Dw-AGCACGAC), a 20mer, d(CCTACGCAAAT-Dw-GGCATCC), and a 30mer, d(CTCGTCAGCATC-Dw-CATCATACAGTCAGTG), in which Dw represents the Dewar valence isomer of the (6–4) photoproduct formed at the TT site, were synthesized on a DNA synthesizer. Since this photoproduct is labile under alkaline conditions (11,22), 2′-deoxyribonucleoside phosphoramidites of N^6-phenoxyacetyladenine, N^4-acetylcytosine and N^2-(4-isopropylphenoxy)acetylguanine, which can be deprotected under mild conditions, were used together with that of unprotected thymine. After the chain assembly, the oligonucleotides were cleaved from the support and deprotected by the treatment with aqueous ammonia at room temperature for 2 h. Analysis of the crude samples of the obtained oligonucleotides was performed by reversed-phase HPLC, as shown in Figure 3A and B. A major peak was obtained in each case, but many peaks of impurities were detected at longer retention times. These impurities were also detected in our previous studies on the (6–4) photoproduct, and they were assumed to be formed by the coupling of the phosphoramidites with the N3 imino function of the 5′ component of the (6–4) photoproduct (25,26,33). Since the 5′ component of the Dewar isomer has the same chemical structure as that of the (6–4) photoproduct, this type of branching side reaction must have occurred. To verify this proposal, as well as to improve the yields of the desired oligonucleotides, the tetrazole was replaced with benzimidazolium triflate (BIT), which was originally used as an activator of phosphoramidites by Hayakawa's group (34,35) and prevented the by-product formation in the synthesis of (6–4) photoproduct-containing oligonucleotides (33). As shown in Figure 3C, the results were improved to a great extent using this alternative activator.

The oligonucleotides were purified by reversed-phase HPLC and the 12mer was analyzed by MALDI-TOF mass spectrometry (Supplementary Figure 3). The calculated and obtained *m/z* values in the negative ion mode were 3611.74 and 3611.94, respectively. The presence of the Dewar photoproduct in the obtained oligonucleotides was demonstrated using the 12mer. In our previous study (12), the same Dewar photoproduct-containing 12mer was prepared by irradiation of the (6–4) photoproduct-containing one, and these two oligonucleotides were separated from each other by reversed-phase HPLC. This experiment was performed using the 12mer synthesized in the present study. As shown in Figure 4A, the 12mer in question coeluted with the Dewar photoproduct-containing 12mer that was used in our previous study (12), whereas it was separated from the (6–4) photoproduct-containing 12mer. Further characterization of the Dewar 12mer was performed using the UV conversion to the (6–4) photoproduct and the enzymatic digestion, as shown in Supplementary Figures 4 and 5, respectively. In

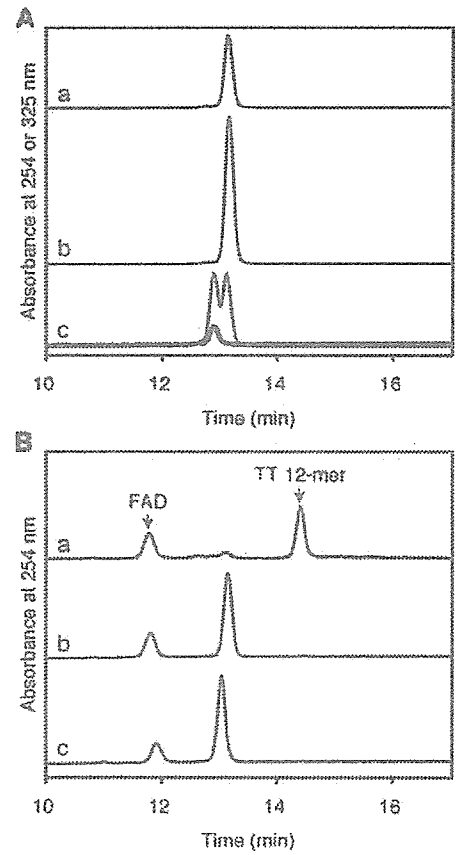

Figure 4. (A) Reversed-phase HPLC analysis of the Dewar 12mer. (a) The 12mer synthesized in this study, (b) co-injection with the Dewar photoproduct-containing 12mer prepared by irradiation of the (6–4) photoproduct-containing 12mer and (c) co-injection with the (6–4) photoproduct-containing 12mer with the same sequence context. The thick and thin lines show the chromatograms monitored at 325 and 254 nm, respectively, and the 325 nm chromatogram is magnified by a factor of 5. (B) Analysis of the (6–4) photolyase reaction with the (6–4) 12mer (a) and the Dewar 12mer (b and c). The reaction times were 3 h (a and b) and 24 h (c). The HPLC conditions are described in Materials and Methods.

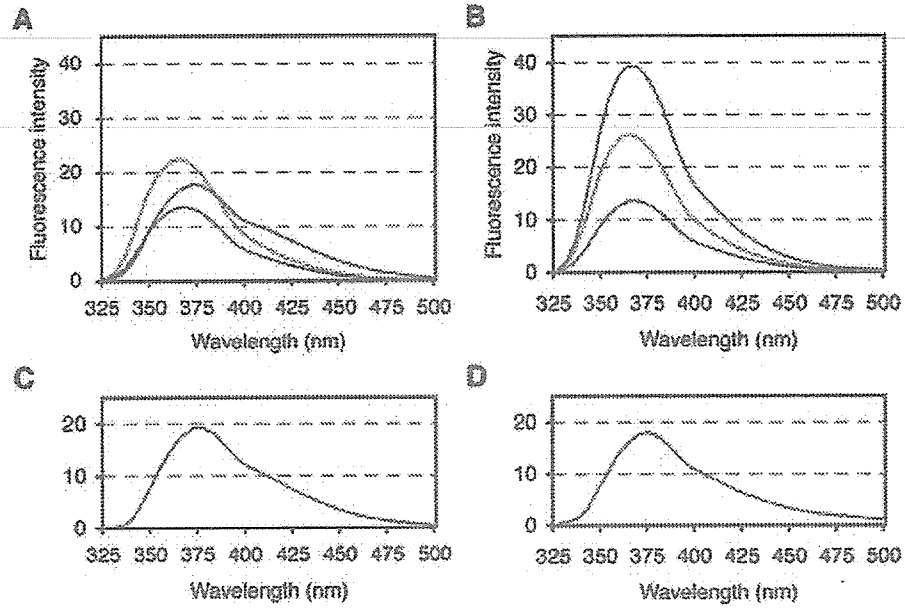

Figure 5. (A and B) Fluorescence emission spectra of the Dewar (red), (6–4) (blue) and TT (green) 20mers hybridized to a complementary strand containing 2-aminopurine in the absence (A) and in the presence (B) of the (6–4) photolyase. (C and D) Fluorescence emission spectra of the (6–4) 20mer hybridized to a complementary strand without 2-aminopurine in the absence (C) and in the presence (D) of the (6–4) photolyase.

the latter experiment, the phosphodiester linkage on the 3′ side of the photoproduct was not cleaved. However, no difference was observed between the oligonucleotide synthesized in this study and the authentic sample prepared by irradiation of the (6–4) photoproduct-containing oligonucleotide, and the presence of the Dewar photoproduct was demonstrated by the UV conversion to the (6–4) photoproduct (trace d in Supplementary Figure 5A). These results show that the Dewar photoproduct-containing oligonucleotides, which are free from contamination with the (6–4) photoproduct-containing oligomers, can be synthesized using the method described here.

Reaction and binding of (6–4) photolyase with Dewar photoproduct-containing oligonucleotides

The (6–4) photolyase was first discovered in a cell extract of *Drosophila melanogaster* (20), and subsequently was found in *X.laevis* (36) and *Arabidopsis thaliana* (37). This enzyme contains flavin adenine dinucleotide (FAD) as a chromophore (36), and the analysis of its reaction strongly suggested that this enzyme repairs the (6–4) photoproducts to their original pyrimidines by utilizing blue to near-UV light (20,38). We demonstrated previously that this enzyme restored the pyrimidines of the (6–4) photoproducts formed at the TT (31) and TC (26) sites to their normal forms, and proposed the repair mechanism of this enzyme (39). Although a crystal structure of CPD photolyase, another enzyme for CPD repair, has been solved in a complex form with its substrate DNA (40), no structural information has been reported for the (6–4) photolyase thus far. In the previous studies, the (6–4) photolyase could bind DNA containing the Dewar photoproduct, but the repair rate was reduced to a great extent when the Dewar photoproduct-containing DNA was used as a substrate (21,31). Therefore, this type of lesion may be useful in the co-crystallization experiments of the (6–4) photolyase.

To test the utility of the Dewar photoproduct-containing DNA, we verified the (6–4) photolyase reaction using the chemically synthesized oligonucleotides. The 12mer containing the Dewar photoproduct, as well as that containing the (6–4) photoproduct in the same sequence context, was treated with *X.laevis* (6–4) photolyase, and the reaction mixtures were analyzed by reversed-phase HPLC. As shown in Figure 4B, the (6–4) 12mer was converted to the undamaged 12mer (TT 12mer) by exposing the reaction mixture to fluorescent lighting for 3 h (trace a), and the repair was confirmed by co-injection of the product with the TT 12mer. In contrast, the peak of the TT 12mer was not detected in the Dewar case (trace b) and prolonged exposure (up to 24 h) did not cause any change (trace c). Since there was a possibility that the above results were obtained by the loss of the affinity of the (6–4) photolyase for the Dewar photoproduct-containing DNA, the enzyme binding was analyzed using a fluorescent base analog, 2-aminopurine. In the case of the CPD photolyase, flipping of the CPD lesion upon enzyme binding was shown by using a complementary strand containing 2-aminopurine (41), and the same mechanism was proposed for the (6–4) photolyase (39). Therefore, this type of experiment was expected to demonstrate the two phenomena, the enzyme binding and the base flipping, simultaneously. The Dewar photoproduct-containing 20mer was hybridized to d(GGATGCC-Ap-AATTTGCGTAGG), in which Ap represents 2-aminopurine. In this duplex, the 2-aminopurine was opposite the 3′ component of the Dewar photoproduct. We changed the position of 2-aminopurine in this sequence context, and the fluorescence intensity observed for the duplex was sometimes close to that of the single-stranded oligonucleotide containing this fluorescent base analog (data not

shown). This type of position effect on the emission of 2-aminopurine has been reported recently for another lesion-containing DNA (42). Using the above-mentioned duplex, as well as the undamaged and (6–4) photoproduct-containing duplexes as negative and positive controls, respectively, fluorescence emission spectra were measured in the absence and presence of the (6–4) photolyase (Figure 5A and B). Since the (6–4) photoproduct is a fluorescent base, emission spectra of the (6–4) photoproduct-containing duplex without 2-aminopurine were measured under the same conditions, to confirm that its fluorescence did not affect this analysis (Figure 5C and D). Moreover, there was a possibility that fluorescence resonance energy transfer might occur between 2-aminopurine and the (6–4) photoproduct, but we confirmed that such an effect was small enough for this experiment (data not shown). An increase of the fluorescence intensity upon the addition of the enzyme was observed for the Dewar photoproduct-containing duplex, but it was much smaller than that observed for the (6–4) photoproduct-containing duplex. These results indicate that the (6–4) photolyase binds the DNA containing the Dewar photoproduct and induces a structural change in DNA to some extent. However, it is suggested that the binding mode is different between the (6–4) photoproduct-containing substrate and the Dewar isomer-containing duplex although the reported affinities of this enzyme for these two types of duplexes are similar (21,31).

We have synthesized a phosphoramidite building block of the Dewar valence isomer of the (6–4) photoproduct formed at the thymidylyl(3′–5′)thymidine site and successfully incorporated it into oligodeoxyribonucleotides. Using these oligonucleotides, the reaction and the binding of the (6–4) photolyase were analyzed, and the results suggested an enzyme binding mode different from the recognition of the original substrate. It is expected that oligonucleotides synthesized by this method will contribute to molecular and structural biology in the field of mutagenesis and DNA repair.

SUPPLEMENTARY DATA

Supplementary data are available at NAR Online.

ACKNOWLEDGEMENTS

The authors thank Dr Hidehito Urata (Osaka University of Pharmaceutical Sciences) for obtaining the high-resolution mass data. This study was supported by a Grant-in-Aid for Scientific Research from the Ministry of Education, Culture, Sports, Science, and Technology, Japan, and a grant from the Asahi Glass Foundation. K.H. was supported by a Research Fellowship of the Japan Society for the Promotion of Science for Young Scientists. Funding to pay the Open Access publication charges for this article was provided by the Asahi Glass Foundation.

Conflict of interest statement. None declared.

REFERENCES

1. Johns,H.E., Pearson,M.L., LeBlanc,J.C. and Helleiner,C.W. (1964) The ultraviolet photochemistry of thymidydyl-(3′→5′)-thymidine. *J. Mol. Biol.*, **9**, 503–524.
2. Taylor,J.-S. and Cohrs,M.P. (1987) DNA, light, and Dewar pyrimidinones: the structure and biological significance of TpT3. *J. Am. Chem. Soc.*, **109**, 2834–2835.
3. Taylor,J.-S., Garrett,D.S. and Cohrs,M.P. (1988) Solution-state structure of the Dewar pyrimidinone photoproduct of thymidydyl-(3′→5′)-thymidine. *Biochemistry*, **27**, 7206–7215.
4. Taylor,J.-S., Lu,H.-F. and Kotyk,J.J. (1990) Quantitative conversion of the (6–4) photoproduct of TpdC to its Dewar valence isomer upon exposure to simulated sunlight. *Photochem. Photobiol.*, **51**, 161–167.
5. Lemaire,D.G.E. and Ruzsicska,B.P. (1993) Quantum yields and secondary photoreactions of the photoproducts of dTpdT, dTpdC and dTpdU. *Photochem. Photobiol.*, **57**, 755–769.
6. Douki,T., Court,M., Sauvaigo,S., Odin,F. and Cadet,J. (2000) Formation of the main UV-induced thymine dimeric lesions within isolated and cellular DNA as measured by high performance liquid chromatography-tandem mass spectrometry. *J. Biol. Chem.*, **275**, 11678–11685.
7. Douki,T. and Cadet,J. (2001) Individual determination of the yield of the main UV-induced dimeric pyrimidine photoproducts in DNA suggests a high mutagenicity of CC photolesions. *Biochemistry*, **40**, 2495–2501.
8. Clingen,P.H., Arlett,C.F., Roza,L., Mori,T., Nikaido,O. and Green,M.H.L. (1995) Induction of cyclobutane pyrimidine dimers, pyrimidine(6–4)pyrimidone photoproducts, and Dewar valence isomers by natural sunlight in normal human mononuclear cells. *Cancer Res.*, **55**, 2245–2248.
9. Perdiz,D., Gróf,P., Mezzina,M., Nikaido,O., Moustacchi,E. and Sage,E. (2000) Distribution and repair of bipyrimidine photoproducts in solar UV-irradiated mammalian cells: possible role of Dewar photoproducts in solar mutagenesis. *J. Biol. Chem.*, **275**, 26732–26742.
10. Douki,T., Reynaud-Angelin,A., Cadet,J. and Sage,E. (2003) Bipyrimidine photoproducts rather than oxidative lesions are the main type of DNA damage involved in the genotoxic effect of solar UVA radiation. *Biochemistry*, **42**, 9221–9226.
11. Kan,L.-S., Voituriez,L. and Cadet,J. (1992) The Dewar valence isomer of the (6–4) photoadduct of thymidylyl-(3′–5′)-thymidine monophosphate: formation, alkaline lability and conformational properties. *J. Photochem. Photobiol. B*, **12**, 339–357.
12. Fujiwara,Y. and Iwai,S. (1997) Thermodynamic studies of the hybridization properties of photolesions in DNA. *Biochemistry*, **36**, 1544–1550.
13. Jing,Y., Kao,J.F.-L. and Taylor,J.-S. (1998) Thermodynamic and base-pairing studies of matched and mismatched DNA dodecamer duplexes containing *cis-syn*, (6-4), and Dewar photoproducts of TT. *Nucleic Acids Res.*, **26**, 3845–3853.
14. LeClerc,J.E., Borden,A. and Lawrence,C.W. (1991) The thymine–thymine pyrimidine–pyrimidone(6-4) ultraviolet light photoproduct is highly mutagenic and specifically induces 3′ thymine-to-cytosine transitions in *Escherichia coli*. *Proc. Natl Acad. Sci. USA*, **88**, 9685–9689.
15. Smith,C.A., Wang,M., Jiang,N., Che,L., Zhao,X. and Taylor,J.-S. (1996) Mutation spectra of M13 vectors containing site-specific cis-syn, trans-syn-I, (6–4), and Dewar pyrimidone photoproducts of thymidylyl-(3′→5′)-thymidine in *Escherichia coli* under SOS conditions. *Biochemistry*, **35**, 4146–4154.
16. Fujiwara,Y., Masutani,C., Mizukoshi,T., Kondo,J., Hanaoka,F. and Iwai,S. (1999) Characterization of DNA recognition by the human UV-damaged DNA-binding protein. *J. Biol. Chem.*, **274**, 20027–20033.
17. Sugasawa,K., Okuda,Y., Saijo,M., Nishi,R., Matsuda,N., Chu,G., Mori,T., Iwai,S., Tanaka,K., Tanaka,K. *et al.* (2005) UV-induced ubiquitylation of XPC protein mediated by UV–DDB–ubiquitin ligase complex. *Cell*, **121**, 387–400.
18. Reardon,J.T., Nichols,A.F., Keeney,S., Smith,C.A., Taylor,J.-S., Linn,S. and Sancar,A. (1993) Comparative analysis of binding of human damaged DNA-binding protein (XPE) and *Escherichia coli* damage recognition protein (UvrA) to the major ultraviolet photoproducts: T[*c,s*]T, T[*t,s*]T, T[6-4]T, and T[Dewar]T. *J. Biol. Chem.*, **268**, 21301–21308.
19. Courdavault,S., Baudouin,C., Charveron,M., Canguilhem,B., Favier,A., Cadet,J. and Douki,T. (2005) Repair of the three main types of bipyrimidine DNA photoproducts in human keratinocytes exposed to UVB and UVA radiations. *DNA Repair*, **4**, 836–844.
20. Todo,T., Takemori,H., Ryo,H., Ihara,M., Matsunaga,T., Nikaido,O., Sato,K. and Nomura,T. (1993) A new photoreactivating enzyme that

specifically repairs ultraviolet light-induced (6-4)photoproducts. *Nature*, **361**, 371–374.
21. Zhao,X., Liu,J., Hsu,D.S., Zhao,S., Taylor,J.-S. and Sancar,A. (1997) Reaction mechanism of (6-4) photolyase. *J. Biol. Chem.*, **272**, 32580–32590.
22. Smith,C.A. and Taylor,J.-S. (1993) Preparation and characterization of a set of deoxyoligonucleotide 49-mers containing site-specific cis-syn, trans-syn-I, (6-4), and Dewar photoproducts of thymidylyl(3′→5′)-thymidine. *J. Biol. Chem.*, **268**, 11143–11151.
23. Taylor,J.-S., Brockie,I.R. and O'Day,C.L. (1987) A building block for the sequence-specific introduction of *cis–syn* thymine dimers into oligonucleotides. Solid-phase synthesis of TpT[c,s]pTpT. *J. Am. Chem. Soc.*, **109**, 6735–6742.
24. Murata,T., Iwai,S. and Ohtsuka,E. (1990) Synthesis and characterization of a substrate for T4 endonuclease V containing a phosphorodithioate linkage at the thymine dimer site. *Nucleic Acids Res.*, **18**, 7279–7286.
25. Iwai,S., Shimizu,M., Kamiya,H. and Ohtsuka,E. (1996) Synthesis of a phosphoramidite coupling unit of the pyrimidine (6–4) pyrimidone photoproduct and its incorporation into oligodeoxynucleotides. *J. Am. Chem. Soc.*, **118**, 7642–7643.
26. Mizukoshi,T., Hitomi,K., Todo,T. and Iwai,S. (1998) Studies on the chemical synthesis of oligonucleotides containing the (6–4) photoproduct of thymine–cytosine and its repair by (6–4) photolyase. *J. Am. Chem. Soc.*, **120**, 10634–10642.
27. Masutani,C., Kusumoto,R., Iwai,S. and Hanaoka,F. (2000) Mechanisms of accurate translesion synthesis by human DNA polymerase η. *EMBO J.*, **19**, 3100–3109.
28. Tissier,A., Frank,E.G., McDonald,J.P., Iwai,S., Hanaoka,F. and Woodgate,R. (2000) Misinsertion and bypass of thymine–thymine dimers by human DNA polymerase ι. *EMBO J.*, **19**, 5259–5266.
29. Ohashi,E., Ogi,T., Kusumoto,R., Iwai,S., Masutani,C., Hanaoka,F. and Ohmori,H. (2000) Error-prone bypass of certain DNA lesions by the human DNA polymerase κ. *Genes Dev.*, **14**, 1589–1594.
30. Seki,M., Masutani,C., Yang,L.W., Schuffert,A., Iwai,S., Bahar,I. and Wood,R.D. (2004) High-efficiency bypass of DNA damage by human DNA polymerase Q. *EMBO J.*, **23**, 4484–4494.
31. Hitomi,K., Kim,S.-T., Iwai,S., Harima,N., Otoshi,E., Ikenaga,M. and Todo,T. (1997) Binding and catalytic properties of *Xenopus* (6–4) photolyase. *J. Biol. Chem.*, **272**, 32591–32598.
32. Taylor,J.-S. (1995) DNA, sunlight and skin cancer. *Pure Appl. Chem.*, **67**, 183–190.
33. Iwai,S., Mizukoshi,T., Fujiwara,Y., Masutani,C., Hanaoka,F. and Hayakawa,Y. (1999) Benzimidazolium triflate-activated synthesis of (6–4) photoproduct-containing oligonucleotides and its application. *Nucleic Acids Res.*, **27**, 2299–2303.
34. Hayakawa,Y., Kataoka,M. and Noyori,R. (1996) Benzimidazolium triflate as an efficient promoter for nucleotide synthesis via the phosphoramidite method. *J. Org. Chem.*, **61**, 7996–7997.
35. Hayakawa,Y. and Kataoka,M. (1998) Facile synthesis of oligodeoxyribonucleotides via the phosphoramidite method without nucleoside base protection. *J. Am. Chem. Soc.*, **120**, 12395–12401.
36. Todo,T., Kim,S.-T., Hitomi,K., Otoshi,E., Inui,T., Morioka,H., Kobayashi,H., Ohtsuka,E., Toh,H. and Ikenaga,M. (1997) Flavin adenine dinucleotide as a chromophore of the *Xenopus* (6–4)photolyase. *Nucleic Acids Res.*, **25**, 764–768.
37. Nakajima,S., Sugiyama,M., Iwai,S., Hitomi,K., Otoshi,E., Kim,S.-T., Jiang,C.-Z., Todo,T., Britt,A.B. and Yamamoto,K. (1998) Cloning and characterization of a gene (*UVR3*) required for photorepair of 6–4 photoproducts in *Arabidopsis thaliana*. *Nucleic Acids Res.*, **26**, 638–644.
38. Kim,S.-T., Malhotra,K., Smith,C.A., Taylor,J.-S. and Sancar,A. (1994) Characterization of (6-4) photoproduct DNA photolyase. *J. Biol. Chem.*, **269**, 8535–8540.
39. Hitomi,K., Nakamura,H., Kim,S.-T., Mizukoshi,T., Ishikawa,T., Iwai,S. and Todo,T. (2001) Role of two histidines in the (6-4) photolyase reaction. *J. Biol. Chem.*, **276**, 10103–10109.
40. Mees,A., Klar,T., Gnau,P., Hennecke,U., Eker,A.P.M., Carell,T. and Essen,L.-O. (2004) Crystal structure of a photolyase bound to a CPD-like DNA lesion after *in situ* repair. *Science*, **306**, 1789–1793.
41. Christine,K.S., MacFarlane,A.W., Yang,K. and Stanley,R.J. (2002) Cyclobutylpyrimidine dimer base flipping by DNA photolyase. *J. Biol. Chem.*, **277**, 38339–38344.
42. Malta,E., Moolenaar,G.F. and Goosen,N. (2006) Base flipping in nucleotide excision repair. *J. Biol. Chem.*, **281**, 2184–2194.

Circadian Intraocular Pressure Rhythm Is Generated by Clock Genes

Ari Maeda,[1] Sosuke Tsujiya,[1] Tomomi Higashide,[1] Kazunori Toida,[2] Takeshi Todo,[3] Tomoko Ueyama,[4] Hitoshi Okamura,[4] and Kazuhisa Sugiyama[1]

Purpose. The present study in a mouse model was undertaken to reveal the role of the circadian clock genes *Cry1* and *Cry2* in generation of 24-hour intraocular pressure (IOP) rhythm.

Methods. IOP was measured at eight time points daily (circadian time [CT] 0, 3, 6, 9, 12, 15, 18, and 21 hours), using a microneedle method in four groups of C57BL/6J mice (groups 1 and 3, wild-type; groups 2 and 4, *Cry*-deficient [$Cry1^{-/-}Cry2^{-/-}$]). During the IOP measurements, mice in groups 1 and 2 were maintained in a 12-hour light–dark cycle (LD), whereas mice in groups 3 and 4 were kept in a constant darkness (DD) that started 24 to 48 hours before the measurements. Circadian IOP variations in each group were evaluated by one-way analysis of variance (ANOVA) and Scheffé tests.

Results. In wild-type mice living in LD conditions, pressures measured in the light phase were significantly lower than those in the dark phase. This daily rhythm was maintained under DD conditions with low pressure in the subjective day and high pressure in the subjective night. In contrast, *Cry*-deficient mice did not show significant circadian changes in IOP, regardless of environmental light conditions.

Conclusions. These findings demonstrate that clock oscillatory mechanisms requiring the activity of core clock genes are essential for the generation of a circadian rhythm of intraocular pressure. (*Invest Ophthalmol Vis Sci.* 2006;47:4050–4052) DOI:10.1167/iovs.06-0183

Previous studies have demonstrated that intraocular pressures (IOPs) of rabbits, rats, chicks, marmosets, and mice have a biphasic pattern when the animals are maintained in a 12-hour light–dark (LD) cycle.[1–5] Because this IOP rhythm in rabbits and rats is maintained in an environment of constant darkness, it has been suggested that day–night IOP variations are related to circadian rhythms in these species.[1,2]

Several factors have been reported to be associated with 24-hour IOP rhythm. Sympathetic nerves are thought to play an important role because neuronal impairment abolishes day–night variations in IOP.[6–9] Other studies have shown that aqueous humor concentrations of norepinephrine and melatonin have 24-hour profiles that are synchronized with changes in IOP.[7,9,10] Furthermore, several adrenergic receptors were also involved in the nocturnal IOP elevation in rabbits based on studies in which topical selective adrenergic agents were used.[9] However, the molecular mechanism that generates 24-hour IOP rhythm remains unknown.

In mammals, circadian oscillation is driven by a transcription–translation-based core feedback loop of a set of clock genes that is dynamically regulated by clock proteins.[11,12] Previous studies have shown that the absence of *Cry1* and *Cry2* genes, members of the family of plant blue-light receptors (cryptochromes), in mice results in complete loss of behavioral rhythm.[13–15] A previous study investigating the effects of lesions of the suprachiasmatic nuclei indicated that the central circadian clock is involved in 24-hour IOP rhythm in rabbits.[16] Therefore, we hypothesized that if the IOP rhythm is controlled by the circadian clock, the rhythm would be abolished in animals genetically deficient in these two clock genes. To examine this hypothesis, we measured circadian IOP changes in *Cry*-deficient ($Cry1^{-/-}Cry2^{-/-}$) mice and compared results with those for wild-type mice.

Materials and Methods

Animals

Four groups of C57BL/6J mice (groups 1 and 3, wild-type; groups 2 and 4, *Cry*-deficient [$Cry1^{-/-}Cry2^{-/-}$]) were used in this study. *Cry*-deficient mice were generated as described previously.[17] Wild-type mice were obtained from a local supplier (Charles River Japan, Inc., Yokohama, Japan). Mice were housed at 23°C with food and water ad libitum. All experiments were performed in compliance with the ARVO Statement for the Use of Animals in Ophthalmic and Vision Research. Initial animal age in each of the four groups ranged from 8 to 12 weeks. Body weight ranged from 25 to 37 g in wild-type mice and 19 to 27 g in *Cry*-deficient mice at the time IOP measurements were begun.

All mice were maintained in a 12-hour LD condition at least 2 weeks before IOP measurements were begun. During the period of IOP measurements, mice in groups 1 and 2 remained in LD conditions, whereas mice in groups 3 and 4 were kept in constant darkness (DD) conditions that started 24 hours before the beginning of measurements.

IOP Measurements

Mice (wild-type, $n = 80$; *Cry*-deficient, $n = 60$) were anesthetized by intraperitoneal injection of ketamine (100 mg/kg) and xylazine (9 mg/kg). IOP was measured by the microneedle method as described previously.[18] Briefly, a glass microneedle was made with a pipette puller and connected to a pressure transducer that was inserted into the anterior chamber through the cornea using a micromanipulator. An IOP measurement for each mouse was obtained for one eye selected at random 4 to 6 minutes after administration of anesthesia when the IOP under anesthesia remained stable.[18]

When IOP measurements were to be performed repeatedly in the same mouse, the interval of measurements was at least 1 week, to avoid any effect of general anesthesia, and the eye to be used for

From the [1]Department of Ophthalmology, Kanazawa University Graduate School of Medical Science, Ishikawa, Japan; the [2]Department of Anatomy and Cell Biology, Institute of Health Biosciences, The University of Tokushima Graduate School, Tokushima, Japan; the [3]Radiation Biology Center, Kyoto University, Kyoto, Japan; and the [4]Division of Molecular Brain Science, Department of Brain Sciences, Kobe University Graduate School of Medicine, Kobe, Japan.

Submitted for publication February 21, 2006; revised April 26, 2006; accepted July 25, 2006.

Disclosure: **A. Maeda**, None; **S. Tsujiya**, None; **T. Higashide**, None; **K. Toida**, None; **T. Todo**, None; **T. Ueyama**, None; **H. Okamura**, None; **K. Sugiyama**, None

The publication costs of this article were defrayed in part by page charge payment. This article must therefore be marked "*advertisement*" in accordance with 18 U.S.C. §1734 solely to indicate this fact.

Corresponding author: Ari Maeda, Department of Ophthalmology, Kanazawa University Graduate School of Medical Science, 13-1 Takaramachi, Kanazawa, Ishikawa 9208641, Japan; ari@p2222.nsk.ne.jp.